Topographic and hydrodynamic controls on barrier retreat and preservation: an example from Dogger Bank, North Sea

Andy R. Emery*[1], David M. Hodgson[1], Natasha L.M. Barlow[1], Jonathan L. Carrivick[2], Carol J. Cotterill[3], Claire L. Mellett[4], Adam D. Booth[1]

*corresponding author, ee06ae@leeds.ac.uk

[1]School of Earth and Environment, University of Leeds, UK

[2]School of Geography, University of Leeds, UK

[3]British Geological Survey, The Lyell Centre, Edinburgh, UK

[4]Wessex Archaeology, Salisbury, UK

0 Abstract

Barrier retreat can occur due to in-place drowning, overstepping or rollover, depending on the interplay of controls such as sea-level rise, sediment supply, coastal hydrodynamic regime and topography. Offshore sedimentary archives of barriers active during rapid Holocene sea-level rise provide important records of marine transgression, which are vital analogues to support appropriate mitigation strategies for future coastal realignment under projected relative sea-level rise scenarios. This study analyses the sedimentary archive at Dogger Bank, which is a formerly-glaciated area in the North Sea. Dogger Bank experienced marine transgression due to Early Holocene rapid relative sea-level rise. An integrated dataset of vibrocores and high-resolution seismic reflection data permits a stratigraphic framework to be established, which reveals the buried coastal geomorphology of the southern Dogger Bank for the first time. A transgressive stratigraphy was identified, comprising a topographically complicated basal glacial and terrestrial succession, overlain by two phases of barrier and tidal mudflat deposition, prior to shallow marine sedimentation. Barrier phase A was a recurved barrier drowned in place, and discontinuously overstepped to barrier phase B, which experienced continuous overstepping. By linking barrier elevations to relative sea-level curves, the timing of each barrier phase was established. Both barrier phases retreated during periods of rapid sea-level rise with abundant sediment supply. Coastal hydrodynamics (increasing wave energy) and antecedent topography with spatially variable accommodation are suggested to be the main reason for differing retreat mechanisms, rather than the rate of sea-level rise. Antecedent coastal geomorphology plays a critical role in erosional and depositional patterns during transgression, and therefore on the timing,

rate and location of marine inundation, which needs to be included in models that aim to forecast hazards in coastal areas.

Keywords: Barrier coast; marine transgression; overstepping; sea level change; Quaternary stratigraphy; Europe

1 Introduction

Considering the projected increase in rates of sea-level rise (e.g. IPCC, 2013), sand or gravel barrier coastlines are increasingly vulnerable to degradation and loss (e.g. Moore and Murray, 2018). Part of the response of barriers to the driver of rapid relative sea-level (RSL) rise includes barrier retreat. Barrier retreat dynamics during RSL rise are a complicated response to the dynamic interplay between rate of RSL rise, sediment supply, coastal hydrodynamic regime, and antecedent topography (Cowell and Thom, 1994; Roy et al., 1994; Swift, 1975, 1968). The geological record offers a valuable archive of past marine transgression that permits investigation of the relationships between RSL rise and barrier retreat style, which could help to inform future mitigation and planning strategies of barrier-protected coastlines.

Different mechanisms of barrier retreat during marine transgression have been identified from preserved barrier systems (Fig. 1). In-place barrier drowning (Fig. 1B) occurs under rapid RSL rise with seaward and landward parts of the barrier preserved (Cattaneo and Steel, 2003; Sanders and Kumar, 1975). Overstepping is a mechanism of retreat in which some back-barrier sediments are preserved (Forbes et al., 1991; Mellett et al., 2012; Mellett and Plater, 2018; Rampino and Sanders, 1980; Storms et al., 2008; Swift et al., 1991), which can be subdivided into “sediment-surplus” (discontinuous; Fig. 1C) and “sediment-deficit” (continuous; Fig. 1D) overstepping (Mellett et al., 2012). Barrier retreat with complete reworking and no preservation, other than a locally developed transgressive lag, is termed rollover (Swift and Moslow, 1982; Leatherman et al., 1983; Fig. 1E).

The need to understand coastal sedimentary process response to RSL rise has led to a focus on (partially) preserved Late Pleistocene and Holocene barriers (Mellett and Plater, 2018). Studies that document barrier preservation of buried or drowned systems have mainly focussed on two-dimensional interpretation of seismic reflection data during a single phase of RSL rise (Browne, 2000; Green et al., 2013; Mellett et al., 2012; Salzmann et al., 2013; Pretorius et al., 2016), or on cemented sandstone barriers (e.g. Albarracín et al., 2013; Gardner et al., 2007, 2005; Green et al., 2013; Jarrett et al., 2005; Roep et al., 1998; Salzmann et al., 2013) with few studies on overstepping of sandy barriers (Cooper et al., 2016; Storms et al., 2008). Furthermore, the widely-employed conceptual and numerical models used to capture barrier retreat mechanisms and preservation have assumed a simple planar underlying topographic surface (e.g. Fig. 1; Storms et al., 2002; Storms et al., 2008; Moore et al., 2010; Mellett et al., 2012; Lorenzo-Trueba and Ashton, 2014; Cooper et al., 2018). However, ice-marginal terrains form complicated antecedent topography (Bennike et al., 2000; Forbes et al., 1995, 1991; Kelley et al., 2010; Shaw et al., 2009), and the style of barrier retreat during marine transgression of these settings is poorly understood.

In this study, the style of barrier retreat in a topographically-complicated setting is deduced by integrating a high-resolution dataset from Dogger Bank, North Sea. Our aim is to describe and explain this site as an extensive offshore palaeo-observatory for the effects of rapid RSL rise during marine transgression. We identify for the first time the coastal geomorphology of a formerly-glaciated terrain during rapid Early Holocene sea-level rise. We review the role of changing hydrodynamics and complex antecedent topography on barrier initiation, retreat, and preservation, and we propose a new conceptual model of topographic influence on barrier retreat.

2 Setting

Dogger Bank is a present-day isolated bathymetric high in the North Sea (Fig. 2) that forms a flat-topped bank between 20 to 30 m below mean sea level (MSL), with the surrounding seabed being 50 to 80 m deep. The origin of the bathymetric high has been variously postulated as a terminal moraine (Belt, 1874) and a sand bank formed by rivers or tidal eddies (Stride, 1959). Initial 1D seismic acquisition (Stride, 1959) combined with piston cores, indicated for the first time that the stratigraphy at Dogger Bank was more complicated than a sandbank. Evidence for glaciation within the North Sea was presented after seabed mapping began in the 1960s and 1970s (Phillips et al., 2017). Advances in marine geological and geophysical data acquisition, such as echo-trace bathymetric profiles, allowed the first identification of glacial landforms and deposits preserved on the seabed (Flinn, 1967; Jansen et al., 1979). Investigations by the British Geological Survey (BGS) during the 1980s and 1990s (Cameron et al., 1992) further proposed a layer-cake stratigraphy of proglacial and glaciomarine sediments for Dogger Bank. Regional seabed mapping and systematic seismic reflection profiling revealed further insights into Quaternary glaciations in the North Sea Basin (Balson and Cameron, 1985; Gibbard et al., 1991; Cameron et al., 1992; Graham et al., 2011; Cotterill et al., 2017a; Phillips et al., 2017).

The BRITICE (Clark et al., 2004) and BRITICE-CHRONO (Clark et al., 2018) studies constrained the timing of the Last Glacial Maximum (LGM) at Dogger Bank to approximately 27 ka cal BP with complete deglaciation of the North Sea by 17 ka BP (Clark et al., 2012). Recent acquisition of high-resolution seismic reflection data and geotechnical boreholes up to 50 m deep in support of windfarm site investigations revealed the complexity of the Dogger Bank stratigraphy as a consequence of its glacial history (Cotterill et al., 2017a). Dogger Bank is now interpreted to be a strongly glaciotectonised composite terminal moraine belt (Carr, 2004; Carr et al., 2006; Cotterill et al., 2017a; Phillips et al., 2018). For the purposes of this study, the most recent, Late Pleistocene and Holocene stratigraphy of Dogger Bank can be simplified into five main formations (Table 1). These represent a transition from glacial (Dogger Bank and Botney Cut Formations), to terrestrial (unnamed fluvial formation), coastal (Elbow Formation) and marine (Nieuw Zeeland Gronden Formation) conditions.

Coastal deposits from the southeast of Dogger Bank were first recovered from vibrocores. Peat containing salt marsh foraminifera and pollen was recovered from vibrocore 213 (Fig. 3), overlain by 4 m of intertidal deposits (Shennan et al., 2000). The basal peat (Fig. 4) was dated to 9130 ± 137 cal BP (Shennan et al., 2000) and provides constraints for Glacio-Isostatic Adjustment (GIA) modelling. RSL curves from various GIA models (Bradley et al., 2011; Kuchar et al., 2012; Shennan et al., 2018, 2006) show that sea level has been rising continuously at Dogger Bank since 17 ka cal BP. Two major periods of increased RSL rise occur, driven by changes in the global ocean volume. The first period occurred during the global meltwater pulse MWP-1A phase (~14.65-14.3 ka; Deschamps et al., 2012), with an average sea-level rise rate of up to 23 mm/yr at Dogger Bank (Bradley et al., 2011; Kuchar et al., 2012; Shennan et al., 2006). The second period occurred at the end of the Younger Dryas, approximately 11.5-10.5 ka, with an average sea-level rise rate of up to 15 mm/yr at Dogger Bank (Bradley et al., 2011; Kuchar et al., 2012; Shennan et al., 2006). It is also possible that a third period of increased rise occurred during the 8.4-8.2 ka sea-level "jump" caused by rapid draining of proglacial lakes Agassiz and Ojibway (Hijma and Cohen, 2010; Törnqvist and Hijma, 2012) or saddle collapse on the Laurentide Ice Sheet (Gregoire et al., 2012; Matero et al., 2017). In the Netherlands, this jump caused an additional 2.11 ± 0.89 m of sea-level rise in 200 years on top of the background rise of 1.95 ± 0.74 m (Hijma and Cohen, 2010). Modelling of the sea-level fingerprint of lake drainage shows a similar magnitude may be expected at Dogger Bank to that experienced in the Netherlands (Törnqvist and Hijma, 2012). However, this sea-level jump is not visible in the modelled RSL curves (e.g. Bradley et al., 2011; Kuchar et al., 2012; Shennan et al., 2018, 2006) as it is below the temporal resolution of the GIA model. Between the short periods of increased rates of RSL rise, the background rate of rise was generally between 5-10 mm/yr. At the end of the Late Pleistocene, the rate was around 5 mm/yr, increasing up to 10 mm/yr during the early Holocene. By the late Holocene, from 7000 cal BP onwards, the RSL rise slowed to less than 5 mm/yr (Bradley et al., 2011; Kuchar et al., 2012; Shennan et al., 2006).

Changes in hydrodynamics under the evolving palaeogeography of the North Sea have been previously modelled (Neill et al., 2010, 2009; Uehara et al., 2006; Ward et al., 2016). The palaeotidal models suggest micro- to mesotidal ranges during the early Holocene, reducing to microtidal by ~6000 BP, and changing little until present day (Uehara et al., 2006; Ward et al., 2016). The tidal current is also modelled to have decreased during the Holocene (Uehara et al., 2006). For the whole of the NW European continental shelf, wave heights are modelled to have increased throughout the Holocene due to increasing fetch (Neill et al., 2009). However, wave energy in the study area is not expected to be significant due to its sheltered location during marine transgression (Brooks et al., 2011; Shennan et al., 2000; Sturt et al., 2013).

3 Methods

An integrated sub-surface dataset of 2D seismic reflection profiles and sediment samples from vibrocores were utilised by this study to understand the evolution of Dogger Bank.

3.1 Vibrocore data

Sediment samples available to this study come from vibrocore data, acquired between 1981 and 1994 by the BGS during marine Regional Mapping Programmes (e.g. Cameron et al., 1992), as well as research programmes such as the Land-Ocean Interaction Study (LOIS; Shennan and Andrews, 2000). The vibrocores recover continuous sections of sediment up to 6 m in length from the seabed (Fig. 3). Generally, the vibrocores are in good condition, although some desiccation and associated fracturing has occurred in some clay-rich sections of core (Fig. 3). Sedimentary facies were identified from the vibrocores based mainly on visual grain size and Munsell colour, but also on composition, texture and grading. Sedimentary structures were rarely observed in vibrocores but were used as diagnostic where present. Sedimentary facies were assigned lithofacies codes based on Evans and Benn (2004). Sediment logs were used to calibrate seismic facies and key seismic stratigraphic surfaces. Vibrocore depth was converted to seismic Two-way Travel time (TWT) using an average velocity of 1600 ms^{-1}, as given by Cotterill et al. (2017b).

3.2 Seismic reflection data interpretation

A dense, 2D grid of shallow seismic reflection data were acquired as part of the site investigation for the Forewind project. A total of 66,000 line km of data were collected, of which 17,000 line km were available in Tranche B for this study (Cotterill et al., 2017a; Fig. 2). 2D lines were spaced every 100 m in the NE-SW orientation and every 500 m in the NW-SE orientation. Seismic data were handled using IHS Kingdom Suite. Two different seismic datasets were used, acquired with sparker and pinger sources. Navigational and acquisition data for the seismic surveys can be found in the supplementary materials. The sparker source allows a maximum depth of investigation of ~150 m (~0.18 s) below the seabed, but with a maximum vertical resolution between 1-2 m. The pinger source offers a vertical resolution of ~0.1 m but with limited, albeit variable, depth penetration. For depths exceeding ~18 m below the seabed (~0.011 s), the pinger-source data lose distinct seismic facies and only high-amplitude reflectors can be distinguished; beyond ~24 m (~0.015 s) below seabed, even high-amplitude events are indistinct against the background noise.

Seismic facies-based interpretation was undertaken, based on Mitchum et al. (1977) and adapted for use with shallow seismic data by Mellett et al. (2013). The pinger-source dataset required some reprocessing, first to approximate the missing negative half-cycles of the wavelet (set to zero in the original records, and therefore lost) and thereafter to suppress surface ghost reflections. Ghosts occur because of interference with reflections from the underside of the sea-surface, and appear in data as seabed-parallel events that obscure genuine reflections within 0.001 s of the seabed. A gentle Ormsby bandpass filter (corner frequencies of 0.8, 1.5 3.5 and 6 kHz) was applied to reconstruct the pinger wavelet. Ghost reflections were suppressed by synchronising the seabed arrivals and then subtracting the average trace of the dataset from individual traces; thereafter, arrivals were returned to their original travel-time. This processing boosts the clarity of surfaces and seismic facies in the pinger data. Seismic facies were correlated with sedimentary facies observed in vibrocores. Pervasive mis-ties were present between the profiles of the pinger data, requiring the definition and application of static corrections, tied for consistency to a single cross-line. Following this processing, the depth of the seabed was corrected using high-resolution multibeam bathymetry data.

Maps generated from interpreting seismic data in two-way time were converted to depth using the P-wave velocities derived from local geotechnical data as well as the velocity of similar sediments recorded regionally in the North Sea, as given by Cotterill et al. (2017b). The sea water velocity was taken to be 1505 m/s and the velocity of the coastal sediments above the Dogger Bank Formation was 1600 m/s (Cotterill et al., 2017b). Individual interpreted seismic horizons were gridded in Kingdom Suite using the flex gridding algorithm, which provides geologically reasonable surfaces.

4 Results

4.1 Sedimentary facies

Eight distinct sedimentary facies were observed and logged in vibrocores. The lithofacies are described in Table 2 and shown correlated across multiple vibrocores in Figure 4, with representative photographs shown in Figure 5.

4.2 Seismic stratigraphy

Seismic interpretation led to the identification of eight distinct seismic units (SUs), based on seismic facies, stratigraphic relationships, and key mappable horizons. Seismic facies were identified from the pinger dataset. The SUs are described in stratigraphic order from the youngest (SU-H) to the oldest (SU-A). Seismic units (Table 3) are shown correlated to vibrocore data in Figure 6 and in broader scale on Figure 7. Due to limitations in seismic data resolution and spatial extent of some seismic units, it is not practical to produce maps of each surface between each seismic unit. Therefore, two key, unconformable, stratigraphic surfaces, horizons S2 and S1, have been identified (Table 3). These surfaces represent major truncating boundaries of underlying deposits.

4.2.1 SU-A

The stratigraphically-oldest seismic unit forms the basal unit to the study area. It is bounded above by horizon S1. Seismic Unit A is generally acoustically transparent. However, occasional, discontinuous, chaotic reflectors of varying amplitude and frequency are present (Fig. 7).

4.2.2 Horizon S1

Horizon S1 (Fig. 8A and 8B) is an unconformity to which younger units are either concordant with, onlap onto, or fill erosion depressions in the surface. It forms a composite, non-planar surface in which a dendritic network of linear channels formed in the northeast. In the south and west, a series of northeast-southwest trending low-amplitude hummocks are evident in the mapped surface (Fig. 8B).

4.2.3 SU-B

SU-B has a distinctive, elongated, mounded geometry and is characterised by a continuous high amplitude top reflector (Fig. 7). Its mounded geometry has not been truncated by the overlying seismic units. Occasional shingled to sigmoidal reflections downlap onto SU-A in a southwesterly direction. The mounds are up to 3 km in length, 200 m wide (Fig. 8C and 8D), and vary in height from very subtle expressions (< 0.001 s, ~0.8 m) up to 0.004 s (~3.3 m).

4.2.4 SU-C

SU-C has a wedge geometry that is thickest in the southeast and pinches out to the northwest (Fig. 6). It shows onlap onto SU-A in the southeast, and downlaps onto SU-A in the northwest. It is only observed at the base of SU-E and not in conjunction with any other seismic unit.

4.2.5 SU-D and SU-E

SU-D and SU-E are both acoustically transparent and are grouped into the same stratigraphic package. SU-E has a lenticular geometry in cross-section, whereas SU-D has a channel form (Fig. 7). SU-D fills incisions into SU-A associated with horizon S1, whereas SU-E is concordant with horizon S1 and onlaps onto SU-C where it is present. Occasional medium-amplitude, continuous reflectors are present in SU-E (Fig. 6). The channel fill of SU-D is mainly transparent, but a draped fill is occasionally observed (Fig. 7).

4.2.6 SU-F

SU-F is observed in a restricted area within the study area. Its external geometry comprises a dipping lens, with the base of the unit shallowing to the northwest (Fig. 7). The sigmoidal to oblique reflectors downlap onto the underlying, acoustically-transparent seismic unit, SU-E and are truncated above by horizon S2.

4.2.7 Horizon S2

Horizon S2 (Fig. 8C and 8D) is a stratigraphic surface with unconformable relationships to the underlying stratigraphy to the northwest and becomes concordant with the stratigraphy in the southeast of the study area. In the northwest of the study area, horizon S2 merges with both horizon S1 and the seabed (Fig. 7). In the southeast of the study area, horizons S2 and S1 become coincident to form a composite surface. In map form, horizon S2 generally dips towards the southeast. However, some ridges trending northeast-southwest are observed in the southeast of the study area, formed by the mounds of seismic unit SU-B (Fig. 8D).

4.2.8 SU-G

SU-G is intermittent throughout the study area, its reflectors parallel with the underlying planar horizon S2. It is rarely thicker than approximately two reflectors (0.0006 s, 50 cm) but appears as very high amplitude, high frequency, even parallel reflectors (Fig. 7).

4.2.9 SU-H

Seismic unit SU-H is the stratigraphically-youngest unit. It is nearly all acoustically transparent, although in some areas, tangential to subparallel oblique, low-frequency, medium amplitude reflectors are observed. It is conformable with SU-G. Its overall geometry is a wedge that pinches out in the northwest and thickens markedly to the southeast.

4.3 Depositional environments

The calibration of seismic facies, geometry, and stratigraphy to vibrocore lithofacies allows for interpretation of the depositional environment to be made. The relationships between seismic facies and lithofacies are shown in Figure 6 and Table 4 and described below. The basal seismic unit, SU-A, is calibrated to two lithofacies, the diamict of Dmm and deformed sands of lithofacies Sd (Fig. 6). No core control exists to calibrate to SU-B. Three lithofacies and three seismic units occur in close stratigraphic succession (Fig. 6). At the base of this succession is a thin peat (< 10 cm) of lithofacies Fpt, which is too thin to be resolved in the seismic data. The only age constraint for the sediment sequence is from this peat, giving an age of 9130 ± 137 cal BP (Shennan et al., 2000). Overlying this is the massive sandy lithofacies Sm_2 that contains chips and clasts of peat, and calibrates with seismic unit SU-C. The massive silty clay lithofacies (Fm) calibrates to the acoustically-transparent seismic unit SU-E, which was deposited contemporaneously with the existence of the channel forms of SU-D. The laminated sand (lithofacies Sl) is a clean, fine sand and calibrates to seismic unit SU-F (Fig. 6). The stratigraphically youngest unit comprises a massive, bioturbated sand (lithofacies Sm_1) and a matrix-supported gravel (Gms) that calibrate to SU-H and SU-G respectively (Fig. 6). These stratigraphic correlations between vibrocore and seismic facies are summarised in Table 4.

4.3.1 Pre-Holocene basement and horizon S1

The diamict is interpreted to be a subglacial diamict of the Dogger Bank Formation (Cotterill et al., 2017a). It is overconsolidated due to glacial loading, and inclusions of sand are indicative of a subglacial till layer that incorporated underlying soft sediments (Evans and Benn, 2004; Menzies, 1990; Van Der Meer et al., 2003). The massive diamict contains no visible evidence of subglacial processes without micromorphological investigation (e.g. Carr et al., 2006). Seismic unit SU-A is generally acoustically transparent to chaotic in nature. Where strong reflectors are seen, they are often steep and discontinuous, suggesting considerable deformation such as imbricate thrust stacking, as well as thrust fault-tip folding, similar to glaciotectonic structure observed in Tranche A to the west (Phillips et al., 2018). Overlying the diamict in the vibrocores are deformed sands (lithofacies Sd). It is not possible to resolve this lithofacies from the diamict on the seismic reflection data. However, based on evidence presented by Cotterill et al. (2017a), this unit is interpreted to be a mixture of glacial outwash plain deposits and loess. Deformation within the sands is interpreted to be periglacial in origin (Cotterill et al., 2017a). Weakly-laminated tidal rhythmites at the base of lithofacies Fm represent the first tidal influence seen above the Pre-Holocene basement. The separating surface between the two units is horizon S1, which is consequently interpreted as the transgressive surface (Cattaneo and Steel, 2003) since it represents the first tidal influence and the interface between terrestrial and marine sediments.

4.3.2 Barrier phase A

Seismic unit SU-B has a mounded, elongate geometry, clear in both profiles and when examined from depth structure maps of the overlying horizon S2 (Fig. 8C, 8D and 9). The southwestern tip of the elongate feature is marked by the ridge orientation rotating by up to 90° towards the northwest. The long axis, running approximately southwest to northeast, is perpendicular to the direction of marine transgression as evidenced by the dip direction of horizon S2. The three-dimensional shape of SU-B, combined with the southwesterly dipping sigmoidal reflectors and the orientation of the recurved direction imply that this unit is a barrier (Fig. 9). The internal structure is similar to the sigmoidal reflectors observed in ground-penetrating radar (GPR) investigations of modern-day barriers (Barboza et al., 2011; Costas et al., 2006; van Heteren et al., 1998). This barrier is termed barrier phase A as it is the stratigraphically-oldest barrier observed, deposited directly onto pre-Holocene basement. Given the transgressive coastal setting, its lower elevation when compared with other barriers in the study area (Fig. 8E) place is as a stratigraphically-older phase of barrier building.

The northwest to southeast orientation of the recurved ends, along with the southwesterly dip direction of the sigmoidal reflections seen in SU-B, imply a longshore drift and sediment transport direction to the southwest during barrier phase A. The shape and scale of the recurved ends (Fig. 9) compares to modern sandy barriers observed on the Lincolnshire (Montreuil and Bullard, 2012) and North Norfolk (Environment Agency, 2013) coasts of the UK. Present-day sediment transport over Dogger Bank is generally from west to east (Houbolt, 1968), but previous models imply this is likely to have changed since the early Holocene during the evolution of the North Sea palaeogeography (Neill et al., 2010, 2009; Uehara et al., 2006). Along the present-day east coast of the UK, sediment transport is generally north to south (e.g. Spurn Head, Yorkshire, Gibraltar Point, Lincolnshire) and east to west (e.g. Blakeney Point, North Norfolk Coast), which support the general transport direction observed during the Holocene barrier phases at Dogger Bank.

4.3.3 Back barrier

A salt marsh environment is interpreted from the presence of lithofacies Fpt, a peat containing salt marsh foraminifera (*Jadaminna macrescens* and *Trochaminna inflata*), abundant foraminiferal test linings, and salt marsh pollen taxa (Shennan et al., 2000). The thin peats formed in the zone between the highest astronomical tide and the mean tide level, and represent the first marine influence on a previously-terrestrial environment. The erosive contact observed between the top of lithofacies Fpt and overlying units is interpreted to represent a local tidal ravinement surface. The wedge of massive, peat-bearing very fine sand of SU-C was deposited above this tidal ravinement surface (Fig. 6 and 7) and thins in a landward direction. The sand is interpreted to be part of a washover fan, with peat fragments entrained during tidal ravinement processes, then reworked during washover. The scale and seismic character of the washover fan is consistent with those observed in GPR investigations of modern transgressive barrier systems (Møller and Anthony, 2003; Tillmann and Wunderlich, 2013). Above this, the massive silty clay was deposited, containing occasional thin sands and peats. The generally fine-grained nature of the observed lithofacies and lack of internal reflectors within seismic units SU-D and SU-E support a low-energy depositional environment. Mapping the channel forms identified in SU-D results in a dendritic to reticulate network (Allen, 2000) that is approximately 3 km wide in the northwest-southeast axis and over 7.5 km long in the northeast-southwest axis, although it continues beyond the study area (Fig. 8B). These channels, comparable in size to Holocene salt marsh creek networks (Allen, 2000), are interpreted to form a tidal creek network, revealed by horizon S1, incised into the Pre-Holocene basement, and may have been inherited from the location of pre-existing channels within the hummocky glacial topography (Fig. 8B). Low-energy, clay-rich lithofacies and the development of a creek network indicate these lithofacies and seismic units to be part of a tidal mudflat, forming at or below mean tide level. Draped reflectors, implying low energy deposition of muds, is also evident (Fig. 6). The presence of salt marsh and tidal mudflat with a washover fan sand imply that the depositional environment for these lithofacies was a back-barrier tidal mudflat.

4.3.4 Barrier phase B

Barrier phase A is separated from a shallower, more landward barrier phase B (Fig. 7 and 8E). An approximate 5 m elevation difference between the two, in addition to an up-dip separating distance of approximately 3 km, makes it likely that barrier phase B is younger and thus can be considered a separate barrier system. An alternative explanation, that barrier phase A and B were components of the same, large barrier system, can be ruled out as it is unlikely that a landward and seaward deposit of a single barrier system would exist coevally, separated by 3 km, on such a small barrier complex. Barriers with multiple components comprising aeolian systems typically are of much larger (tens of kilometre) scales (Bateman et al., 2011; Oliver et al., 2018).

The laminated sand lithofacies (Sl, SU-F) of barrier phase B is well sorted, and texturally and compositionally mature, implying extensive reworking of the sediment. The basal part of the succession is laminated and has intercalated thin peats, implying a low-energy setting into which the overlying, more energetically-deposited fine sands of barrier phase B prograded. The oblique, landward-dipping reflectors that downlap onto the underlying stratigraphy indicate a landward transport of sediment (Fig. 10). The laminated clean sand and distinct seismic facies combined are therefore interpreted to be a back-barrier shoreline, where the barrier retreated onto the back-barrier tidal mudflat (Fig. 10). This unit is stratigraphically separated from barrier phase A (Fig. 7 and 8), and is termed barrier phase B. Since the original morphology of barrier phase B is not preserved, it is not possible to comment on its conformity to morphometric models (e.g. Hayes, 1979; Mulhern et al., 2017) and no further information on sediment transport direction can be interpreted from the data.

4.3.5 Shallow marine

Lithofacies Sm_1 is a texturally and compositionally mature, clean sand with disarticulated shells and shell fragments, interpreted to be a shallow marine sand. Its intense bioturbation supports a lower shoreface to offshore environment of deposition (Dashtgard et al., 2012). The presence of a matrix-supported gravel (Gms, SU-G) at the base of the shallow marine sand is interpreted as a transgressive gravel lag, containing gravel reworked from erosion of underlying glaciogenic deposits through wave ravinement processes. The sand matrix in the gravel lag is similar in mineralogy and grain size to the overlying shoreface sands (Sm_1, SU-H). The gravel lag is not a consistent thickness throughout the area (Fig. 6 and 7). This may be due to localised accumulation of gravel due to fluctuations in gravel supply and wave energy during transgression (e.g. Goff et al., 2010). Overall, the base of the shallow marine unit dips towards the southeast (Fig. 8C and 8D), which corresponds to the northwest direction of wave ravinement during marine transgression. The base of this unit forms horizon S2, which is a composite surface. To the southeast of barrier phase A (Fig. 8D), horizon S2 is a flooding surface (Cattaneo and Steel, 2003), representing transgression with minimal wave ravinement, since there appears to be little erosion and reworking, as no truncation of the glacial deposits is evident. (Fig. 7 and 8). To the northwest of barrier phase A, previous deposits, such as moraine ridges of SU-A (Fig. 8A and 8B), have been eroded, and can be correlated to the truncation of barrier phase B by the same surface, resulting in horizon S2 being interpreted as a wave ravinement surface, in combination with the observed transgressive lag (Cattaneo and Steel, 2003; Zecchin and Catuneanu, 2013).

4.4 Model of coastal evolution

Coastal evolution at Dogger Bank has been split into six stages of landscape evolution (Fig. 12) that incorporates the transition from glacial, through the two barrier phases, to present-day, fully-marine conditions. In the absence of direct chronological control, we estimate the age of the barriers from their preserved elevation, as per Mellett et al. (2012), and compare it to the elevation of RSL at this location predicted by GIA modelling (Kuchar et al., 2012). Constraining the elevation at which a barrier formed with respect to a tidal datum (termed the indicative meaning; Hijma et al., 2015; Shennan, 1982; van de Plassche, 1986), is challenging due to hydrodynamic and weather conditions affecting elevations of base and crest (Kelsey, 2015; Orford et al., 2003). In the absence of defined geomorphological markers such as beach ridges (Kelsey, 2015) or stratigraphic horizons such as tidal flat/salt marsh sediments, we take the elevations of barrier initiation and breakdown preserved in barrier morphology as the height of MSL.

The age of barrier phase A is based on the elevation of its preserved mound morphology. The maximum elevation, and therefore the youngest age that barrier phase A was present, is based on the crest elevation of the mound. The maximum crest height of -32 m OD is 3 m above the lower bounding surface (horizon S1, Fig. 8E) of -35 m OD. At the modern-day North Norfolk coast, which has a similar tidal range and wave regime to Dogger Bank during the Holocene (Neill et al., 2009; Uehara et al., 2006), barriers such as Blakeney Point have a mean crest elevation of 5-6 m above MSL (Environment Agency, 2013). Comparing barrier phase A to this analogue, MSL could be up to 6 m below the maximum crest height of -32 m, giving a MSL of -38 m OD. This estimate is based on a number of reasonable assumptions: that little reworking of the barrier has taken place, which is likely given the intact nature of the barrier morphology; the preserved barrier represents the final stage of its evolution, most likely a part of the breakdown phase when the barrier became drowned; and the crest elevation is related to MSL and not heavily modified by storms and aeolian decoration (Orford et al., 2003). The MSL elevation range of barrier phase A is therefore -38 m to -32 m OD, which, when compared to the RSL curve in Figure 11, suggests an age of c. 10 – 9.3 ka for barrier phase A (Kuchar et al., 2012).

The formation elevation of barrier phase B may be constrained a little further, as the back-barrier overstep downlaps onto the tidal mudflat, which typically occurs between the Lowest Astronomical Tide (LAT) and MSL (Allen, 2000). The back-barrier base here likely formed at or around MSL, meaning uncertainty of the elevation of the crest height does not need to be taken into consideration. We therefore assume an elevation of formation at the barrier-mudflat transition as being between MSL and LAT, which given the tidal range at this time is likely 0.5 - 1 m (Table 5; Uehara et al., 2006; Ward et al., 2016). The barrier phase B base in the seismic data gives an elevation range of -32 to -27 m OD (Fig. 10). Comparing these elevations against the modelled RSL, we estimate an approximate age range for barrier phase B of c. 9.3 – 8.7 ka (Fig. 11; Kuchar et al. 2012).

4.4.1 Stage 1 – Antecedent topography and initial barrier phase A

Immediately following the withdrawal of the Eurasian Ice Sheet from Dogger Bank, around 23 ka BP (Clark et al., 2012; Hughes et al., 2016; Roberts et al., 2018), Dogger Bank was left as a series of ridges, formed as a composite terminal moraine system (Phillips et al., 2018), with basins between moraine ridges filled by glacial outwash. The small-scale topography of the top surface of the larger-scale moraine ridges was hummocky (Fig. 8B), and was subjected to limited and localised modification by fluvial processes during periglacial conditions. Marine transgression of the wider Dogger Bank and Oyster Ground area from the south first occurred during the Younger Dryas at c. 12 ka BP (Fig. 11; Brooks et al., 2011; Sturt et al., 2013). The presence of barrier phase A (SU-G) and the tidal creek system revealed by horizon S1 are the oldest identified coastal landforms. At this stage, c. 10 - 9.3 ka (Fig. 11), barrier development was initiated, and it continued to grow through longshore sediment supply in a southwesterly direction, as shown from the direction of longshore drift (Fig. 9). The contemporaneous development of tidal mudflats (Fm, SU-E) occurred behind the barrier, with some tidal creeks potentially exploiting former terrestrial drainage channels at low points in the hummocky moraine topography (Fig. 8 and 12).

4.4.2 Stage 2 – Barrier phase A drowning

The lack of significant wave ravinement of barrier phase A implies the barrier was drowned in place with minimal reworking, preserving both its seaward and landward faces. Barrier phase A has a low-angle (0.017°) antecedent topography. A hummocky moraine ridge (SU-A) existed between barrier phase A and B (Fig. 8E), which experienced wave ravinement and truncation during ongoing marine transgression (Fig. 12). This ridge may have been the site of initiation of another barrier after barrier phase A drowned, but wave ravinement has removed any evidence of any barrier existing at that location.

4.4.3 Stage 3 – Migration to barrier phase B

A barrier (Sl, SU-F) initiated above the tidal mudflat (Fm, SU-E) deposits to the northwest of the moraine ridge, which had been partially eroded and reworked through wave ravinement (Fig. 12). This barrier either represents a discontinuous landward migration of the barrier with little to no reworking of the previous barrier, termed sediment-surplus overstepping (Fig. 1; Mellett et al., 2012) or initiation of a new barrier following wave ravinement and truncation of the hummocky moraine ridge. The initial location of the phase B barrier is inferred from the most seaward location of the barrier preservation (Fig. 10). This barrier initiated and existed between c. 9.3 and 8.7 ka (Fig. 11).

4.4.4 Stage 4 – barrier overstepping

As sea level continued to rise, barrier phase B migrated landwards. The preservation of landward-facing barrier deposits of phase B, without preservation of seaward barrier faces, implies that the mechanism of barrier retreat was sediment-deficit overstepping (Mellett et al., 2012), also known as overstepping with low preservation (Mellett and Plater, 2018). As the barrier migrated into the back-barrier tidal mudflat basin, the landward faces of the barrier were preserved through continuous overstepping. The seaward barrier faces were removed through wave ravinement during ongoing barrier retreat.

4.4.5 Stage 5 – continued transgression and ravinement

In the northwest of the study area, it is not possible to say whether the barrier rolled over to a new location as horizons S1 and S2 become coincident (Fig. 7), and no further coastal sediments are preserved. Further northwest, beyond the study area, S1 and S2 are coincident with the seabed, preventing further tracking of marine transgression in a landward direction. Continuing transgression and wave ravinement, as picked out by horizon S2 (Fig. 8), has truncated previous barrier and coastal deposits as well as areas where former pre-coastal topography (defined by horizon S1) was present at the coastline, constraining deposition and preservation of coastal sediments (Fig. 12). When compared to the RSL curves for the study area, the elevation of the wave ravinement surface implies transgression occurred prior to the 8.4-8.2 ka sea-level jump (Fig. 11). During the jump, the sea level may have risen as much as 4 m in 200 years (Hijma and Cohen, 2010). This sudden increase in sea level without marked increase in sediment supply may have caused the barrier system to collapse, followed by wave ravinement processes. Because of the broader-scale topography of Dogger Bank at this time, this jump may have resulted in abandonment of coastal systems and a complete transgression over the entire island.

4.4.6 Stage 6 – shallow marine deposition

Coastal evolution stage 6 represents complete inundation of Dogger Bank (Fig. 12). The wave ravinement surface associated with complete transgression (Stage 5) has been buried with shallow marine sand (Sm_1, SU-H), up to a thickness of 13 m in the southeast of the study area (Fig. 7). Limited seismic facies information preserved within the shallow marine sand hinders interpretation of seabed processes such as sediment transport direction. However, large scours observed at the modern-day seabed imply a current direction from west to east, which supports the inferred transport direction from eastward-dipping sigmoidal reflectors that are infrequently seen within the seismic data. This sediment transport direction is also supported by observations and models of currents in the present day and recent North Sea (Davies and Furnes, 1980; Houbolt, 1968; Neill et al., 2010; Uehara et al., 2006).

5 Discussion

5.1 Barrier initiation

Oyster Ground provides a possible initial location for barrier development because it is a large, flat-bottomed basin to the southeast of Dogger Bank (Fig. 2). Furthermore, it is at a similar elevation to the estimated height of sea level during barrier phase A (Fig. 11). During Holocene RSL rise, marine inundation towards the study area was initiated through the Outer Silver Pit (Fig. 2) and into the Oyster Ground embayment (Brooks et al., 2011; Shennan et al., 2000; Sturt et al., 2013). The low-lying, shallow topography of Oyster Ground would have allowed for the accumulation of shallow marine sediments from surrounding terrestrial sources, such as from major European rivers to the south (Gibbard and Lewin, 2016), and from reworking of glaciogenic sediments. Given the large amount of shallow marine sediment available in a large, shallow embayment with a low slope angle (0.001°, taken from bathymetry data in Fig. 2), a barrier system could have initiated even during the rapid rates of RSL rise (~11 mm/year from GIA models, Fig. 11) at this time. Most observations of Holocene barrier formation worldwide require a period of sea-level stillstand or “slowstand” (Billy et al., 2018; Forbes et al., 1995; Green et al., 2013; Kelley et al., 2010; Novak, 2002; Salzmann et al., 2013), or a reduction in the rate of sea-level rise (Brooks et al., 2003). However, barriers may form even during rapid periods of RSL rise if sediment supply is high enough, such as areas rich in glaciogenic sediments (Jensen and Stecher, 1992; Mellett et al., 2012; Shaw et al., 2009).

5.2 Influences on barrier retreat mechanisms

The style of barrier migration during marine transgression is controlled by the balance between barrier forcing mechanisms and factors that affect its potential for migration, termed inertia (Cowell et al., 1991; Cowell and Thom, 1994; Mellett and Plater, 2018; Roy et al., 1994). Barrier retreat and migration is driven by sea-level rise and controlled (forced) by coastal hydrodynamics, as well as the effect of high-energy events such as storms and tsunami. Factors affecting barrier inertia are grain size, sediment supply and topography (Cowell and Thom, 1994). Barrier phases A and B present differing modes of overstepping in response to their specific relative forcing and inertia, summarised in Table 5.

5.2.1 Barrier phase A

During the development of barrier phase A, (c. 10 - 9.3 ka) the rate of RSL rise was high, but decreasing (from 11 mm/year to 9mm/year; Fig. 11; Table 5). However, a low wave energy regime, due to the enclosed embayment and low fetch of the Oyster Ground during that time, is likely to have resulted in a shallow fair-weather wave base responsible for limited reworking and ravinement during transgression (Cattaneo and Steel, 2003; Mellett and Plater, 2018).

High barrier inertia factors likely contributed to the breakdown and migration of barrier phase A. Although the grain size is unknown, the high amplitude reflector seen in the seismic data (Fig. 7) suggests that the barrier may consist of gravel, as seen in seismic profiles of Mellett et al. (2012), which would contribute towards high barrier inertia (Cowell et al., 1991; Roy et al., 1994). High barrier inertia is also supported by the low-complexity, low-relief topography surrounding the barrier location (0.017° gradient perpendicular to the coastline; Fig. 7 and 8) as well as a sudden increase in accommodation within the ~1.5 km-broad back-barrier area.

The strong barrier forcing and inertia factors during the breakdown and migration of barrier phase A have resulted in its drowning in place. Despite high sediment availability, overstepping to a new barrier location was discontinuous due to the low-relief topography that caused a rapid landward migration, driven by rapid RSL rise. The new barrier location was not preserved, but is likely to have been at a point of change in slope, where it may have been topographically pinned on top of the eroded hummocky moraine topography to the northwest of barrier phase A (Fig. 8).

5.2.2 Barrier phase B

Barrier phase B occurred between c. 9.3 – 8.7 ka with an associated rate of RSL rise of ~10 mm/yr (Fig. 11; Table 5). Tidal and wave modelling suggests that barrier phase B was in place during a meso- to microtidal regime (Uehara et al., 2006; Ward et al., 2016) with an increase in wave energy relative to barrier phase A (Neill et al., 2009). The increase in fetch due to increased marine inundation and its associated increase in wave energy would have resulted in a deepening of the fair-weather wave base and an increase in ravinement effectiveness. These factors resulted in strong barrier forcing conditions at this time compared to the period of barrier phase A migration, with a similar driver of rapid RSL rise.

Barrier inertial conditions were generally lower during barrier phase B than barrier phase A. The back-barrier deposits imply that the barrier was composed of sand, which has lower barrier inertia than gravel. Local sediment supply is likely to have been high due to the availability of reworked glaciogenic sediments and the previous, more seaward barrier deposits. The topography of the back-barrier basin into which the barrier was retreating becomes steeper (gradient of 0.046°; Fig. 8) and has channels and antecedent topographic ridges, resulting in highly variable accommodation conditions for the overstepping barrier. This variable back barrier accommodation also enhanced the partial preservation, as opposed to complete reworking, of barrier phase B (Fig. 7).

Because of lower barrier inertia (higher slope angle and smaller grain size) during strong barrier forcing conditions (Table 5), the barrier retreated continuously at a reduced horizontal rate when compared to barrier phase A. However, as initial sediment supply is likely to have been high, the complex, steeper antecedent topography, and associated relatively high local accommodation, is interpreted to be the primary factor in controlling the continuous retreat of barrier phase B. This will have allowed the barrier to be constantly present during migration.

5.2.3 Role of antecedent topography on barrier retreat and preservation

The subglacial conditions in the Dogger Bank area resulted in a set of curved moraine ridges with a hummocky top surface (Phillips et al., 2018) that impacted the style of barrier dynamics during marine inundation in an otherwise low-lying coastal plain area. Barrier phase A was drowned in place. In-place drowning may occur when the rate of sea-level rise is high and/or sediment supply is low (Cattaneo and Steel, 2003), so that the barrier is not reworked during drowning, and the barrier cannot migrate due to low sediment supply. In this scenario, the rate of RSL rise is high (Fig. 11), and sediment supply is assumed to be high due to the availability of reworked glaciogenic sediments and fluvial input into the Oyster Ground (Gibbard and Lewin, 2016). However, the antecedent topography at the barrier phase A location has a low relief (~0.017°), as shown by horizon S1 (Fig. 7 and 8). Antecedent topography may have thus played a role in exacerbating the effect of drowning in place.

Barrier phase B is preserved as landward-dipping barrier sands, truncated by wave ravinement processes. Previous interpretations of Holocene barrier preservation have invoked resilience due to gravel-grade sediment (e.g. Forbes et al., 1991; Jensen and Stecher, 1992; Forbes et al., 1995; Kelley et al., 2010; Mellett et al., 2012; Billy et al., 2018) or early cementation in warmer climates (e.g. Jarrett et al., 2005; Green et al., 2012; Albarracín et al., 2013; Green et al., 2013; Salzmann et al., 2013; Green et al., 2018). Barrier phase B is a rare example of a well-preserved sand barrier that fits neither of these models. Its preservation may in part be due to its position within an embayment (Fig. 12), as observed by Cooper et al. (2016). High accommodation in the back-barrier basin, combined with a steep wave ravinement surface due to low barrier inertia under low barrier forcing conditions, leads to a larger volume of barrier sand being preserved. The steep run-up (0.12°; Fig. 8E) and the presence of topographic highpoints within the back-barrier basin may have also locally altered hydrodynamics to reduce reworking and further enhance barrier preservation (Fig. 13). Numerical models of barrier retreat assume simple topography with planar seaward surfaces (e.g. Storms et al., 2002; Storms et al., 2008; Moore et al., 2010; Lorenzo-Trueba and Ashton, 2014), but more realistic topography should be incorporated into future experiments. Final drowning and minimal ravinement of barrier phase B may have been caused by the sudden increase in the rate of RSL rise due to the 8.4-8.2 ka sea-level jump (Fig. 11).

5.3 Comparison of barrier phases and controls on retreat

The role of coastal hydrodynamics in barrier retreat is rarely studied due to lack of geological proxies for wave and tidal regime, or a lack of modelling (Mellett and Plater, 2018). However, due to previous studies of Holocene hydrodynamic properties through time (e.g. Uehara et al., 2006; Neill et al., 2009; Neill et al., 2010; Ward et al., 2016), we can consider their role in a relative sense, as shown in Table 5. Barrier phase A experienced low barrier forcing and high barrier inertia, whereas barrier phase B experienced higher barrier forcing with lower barrier inertia (Fig. 13). Discontinuous barrier overstepping observed for barrier phase A is similar to that observed in various locations globally (e.g. Brooks et al., 2003; Yang et al., 2006; Storms et al., 2008; Mellett et al., 2012; Pretorius et al., 2016) where a rapid increase in RSL rise rate alone is invoked to explain the discontinuous overstepping. Continuous overstepping, characterised by overlapping back-barrier beach deposits downlapping onto and retrograding into the back-barrier basin, as observed during barrier phase B, is also observed in many transgressed barrier systems (Browne, 2000; Forbes et al., 1991; Mellett et al., 2012). During both phases, RSL rise was rapid. This implies that the rate of RSL rise is a driver of retreat, but less of a control on retreat mechanism than other factors. Sediment supply appears to have been abundant throughout the Holocene, allowing barriers to form despite high rates of RSL rise.

Through qualitative comparison of factors of forcing and inertia (Table 5), the most important controls on barrier retreat at Dogger Bank, under a driver of a similar rate of RSL rise, are therefore the evolving hydrodynamic regime and difference in antecedent topography angle between the two barrier phases (Fig. 13). Qualitative assessment of barrier forcing and inertia may be useful as an assessment of relative controls of barrier retreat, but quantitative assessment of Holocene forcing and inertia mechanisms would provide valuable inputs into modelling future barrier morphodynamics under projected sea-level rise. Further work is needed to explore how quantitative assessment of Holocene barrier forcing and inertia may be undertaken.

6 Conclusions

Vibrocore analysis at Dogger Bank revealed a barrier complex and tidal mudflat sedimentary environment. Calibration of lithofacies to seismic facies reveal the stratigraphic relationship and geomorphological evolution where barriers retreated landwards during marine transgression. Two styles of barrier retreat are observed. Barrier phase A has a distinct, recurved morphology and internally shows progradation due to a northeast to southwest longshore drift direction. Barrier phase A was drowned in place due to rapid sea-level rise and low gradient of the underlying topography, and overstepped discontinuously to a more landward location. Barrier phase B experienced greater forcing conditions, still being driven by a rapid RSL rise, due to the increase in wave energy since barrier phase A, but retreated over a steeper antecedent topography. This caused barrier phase B to retreat by continuous overstepping.

The rate of sea-level rise is similar in both barrier phases, despite them being geomorphologically distinct. RSL rise is an important driver of barrier retreat, but does not control the mechanism of retreat. The most important controls on barrier retreat style are changing coastal hydrodynamics and antecedent topography formed from previous glacial processes. Topography is also a strong control on barrier initiation and preservation processes. Barrier initiation was possible despite rapid inundation of the flat-lying topography of Oyster Ground, combined with likely abundant sediment supply from glaciogenic sediments and fluvial input, allowing a barrier to form under low hydrodynamic energy conditions. This flat-lying topography was also key in drowning barrier phase A in place. The hummocky moraine topography to the northwest of barrier phase A formed an embayment, which potentially increased the preservation of barrier phase B, combined with a steeper run-up and wave ravinement surface.

Despite the qualitative comparison undertaken in this study, quantifying the relative contribution of barrier forcing and inertia on barrier retreat remains difficult to elucidate. Data-rich Dogger Bank provides a well-constrained, important site to test models of barrier evolution under RSL rise in three dimensions. This qualitative study emphasises the need to include large-scale changing topographic configurations and coastal hydrodynamics in forecasts of coastal realignment. The control of topography and hydrodynamics on barrier retreat is particularly important when considering barrier retreat on paraglacial coastlines globally, such as the need to protect infrastructure on coastlines of North America and northwest Europe. In particular, models of landscape response to future sea-level rise should include variability of antecedent topography, as well as evolving hydrodynamics.

7 Declarations of interest

None.

8 Acknowledgements

This study was undertaken as part of a studentship funded by the Leeds Anniversary Research Scholarships. Forewind and the British Geological Survey are thanked for provision of the data and permission to publish. Dr. Sarah Bradley (TU Delft) is thanked for providing RSL curves from her published glacio-isostatic adjustment models, as well as useful discussions on Holocene sea-level change. ARE acknowledges the support of the Quaternary Research Association, the British Sedimentological Research Group and the British Society for Geomorphology for supporting earlier presentation of this work. This paper forms a contribution to the QRA Sea Level and Coastal Change working group. The editor, Professor Edward Anthony, and Professor Andy Green and one anonymous reviewer are thanked for their clear, comprehensive and constructive reviews that led to the improvement of this manuscript.

9 References

Albarracín, S., Alcántara-Carrió, J., Barranco, A., Sánchez García, M.J., Fontán Bouzas, Á., Rey Salgado, J., 2013. Seismic evidence for the preservation of several stacked Pleistocene coastal barrier/lagoon systems on the Gulf of Valencia continental shelf (western Mediterranean). Geo-Marine Lett. 33, 217–223. https://doi.org/10.1007/s00367-012-0315-x

Allen, J.R.L., 2000. Morphodynamics of Holocene salt marshes: A review sketch from the Atlantic and Southern North Sea coasts of Europe. Quat. Sci. Rev. 19, 1155–1231. https://doi.org/10.1016/S0277-3791(99)00034-7

Balson, P., Cameron, T., 1985. Quaternary mapping offshore East Anglia. Mod. Geol. 9, 221–239.

Barboza, E.G., Rosa, M.L.C.C., Hesp, P.A., Dillenburg, S.R., Tomazelli, L.J., Ayup-Zouain, R.N., 2011. Evolution of the Holocene Coastal Barrier of Pelotas Basin (Southern Brazil) - a new approach with GPR data. J. Coast. Res. SI 64 646–650.

Bateman, M.D., Carr, A.S., Dunajko, A.C., Holmes, P.J., Roberts, D.L., McLaren, S.J., Bryant, R.G., Marker, M.E., Murray-Wallace, C. V., 2011. The evolution of coastal barrier systems: A case study of the Middle-Late Pleistocene Wilderness barriers, South Africa. Quat. Sci. Rev. 30, 63–81. https://doi.org/10.1016/j.quascirev.2010.10.003

Belt, T., 1874. An examination of the theories that have been proposed to account for the climate of the glacial period. Q. J. Sci. 421–464.

Bennike, O., Jensen, J.B., Konradi, P.B., Lemke, W., Heinemeier, J., 2000. Early Holocene drowned lagoonal deposits from the Kattegat, southern Scandinavia. Boreas 29, 272–286. https://doi.org/10.1111/j.1502-3885.2000.tb01210.x

Billy, J., Robin, N., Hein, C.J., FitzGerald, D.M., Certain, R., 2018. Impact of relative sea-level changes since the last deglaciation on the formation of a composite paraglacial barrier. Mar. Geol. 400, 76–93. https://doi.org/10.1016/j.margeo.2018.03.009

Bradley, S.L., Milne, G.A., Shennan, I., Edwards, R., 2011. An improved glacial isostatic adjustment model for the British Isles. J. Quat. Sci. 26, 541–552. https://doi.org/10.1002/jqs.1481

Brooks, A.J., Bradley, S.L., Edwards, R.J., Goodwyn, N., 2011. The Palaeogeography of Northwest Europe during the last 20,000 years. J. Maps 5647, 573–587. https://doi.org/10.4113/jom.2011.1160

Brooks, G.R., Doyle, L.J., Suthard, B.C., Locker, S.D., Hine, A.C., 2003. Facies architecture of the mixed carbonate/siliciclastic inner continental shelf of west-central Florida: Implications for Holocene barrier development. Mar. Geol. 200, 325–349. https://doi.org/10.1016/S0025-3227(03)00190-7

Browne, I., 2000. Seismic stratigraphy and relict coastal sediments off the east coast of Australia. Mar. Geol. 121, 81–107.

Cameron, T., Crosby, A., Balson, P., Jeffery, D.H., Lott, G.K., Bulat, J., Harrison, D.J., 1992. United Kingdom offshore regional report: the geology of the southern North Sea. HMSO, London.

Carr, S.J., 2004. The North Sea Basin, in: Ehlers, J., Gibbard, P.L. (Eds.), Quaternary Glaciations - Extent and Chronlogy: Part I: Europe. Elsevier, pp. 261–270.

Carr, S.J., Holmes, R., van der Meer, J.J.M., Rose, J., 2006. The Last Glacial Maximum in the North Sea Basin: Micromorphological evidence of extensive glaciation. J. Quat. Sci. 21, 131–153. https://doi.org/10.1002/jqs.950

Cattaneo, A., Steel, R.J., 2003. Transgressive deposits: A review of their variability. Earth-Science Rev. 62, 187–228. https://doi.org/10.1016/S0012-8252(02)00134-4

Clark, C.D., Ely, J.C., Greenwood, S.L., Hughes, A.L.C., Meehan, R., Barr, I.D., Bateman, M.D., Bradwell, T., Doole, J., Evans, D.J.A., Jordan, C.J., Monteys, X., Pellicer, X.M., Sheehy, M., 2018. BRITICE Glacial Map, version 2: a map and GIS database of glacial landforms of the last British-Irish Ice Sheet. Boreas 47, 11-e8. https://doi.org/10.1111/bor.12273

Clark, C.D., Evans, D.J.A., Khatwa, A., Bradwell, T., Jordan, C.J., Marsh, S.H., Mitchell, W.A., Bateman, M.D., 2004. Map and GIS database of glacial landforms and features related to the last British Ice Sheet. Boreas 33, 359–375. https://doi.org/10.1111/j.1502-3885.2004.tb01246.x

Clark, C.D., Hughes, A.L.C., Greenwood, S.L., Jordan, C., Sejrup, H.P., 2012. Pattern and timing of retreat of the last British-Irish Ice Sheet. Quat. Sci. Rev. 44, 112–146. https://doi.org/10.1016/j.quascirev.2010.07.019

Cooper, J.A.G., Green, A.N., Loureiro, C., 2018. Geological constraints on mesoscale coastal barrier behaviour. Glob. Planet. Change 168, 15–34. https://doi.org/10.1016/j.gloplacha.2018.06.006

Cooper, J.A.G., Green, A.N., Meireles, R.P., Klein, A.H.F., Souza, J., Toldo, E.E., 2016. Sandy barrier overstepping and preservation linked to rapid sea level rise and geological setting. Mar. Geol. 382, 80–91. https://doi.org/10.1016/j.margeo.2016.10.003

Costas, S., Alejo, I., Rial, F., Lorenzo, H., Nombela, M.A., 2006. Cyclical Evolution of a Modern Transgressive Sand Barrier in Northwestern Spain Elucidated by GPR and Aerial Photos. J. Sediment. Res. 76, 1077–1092. https://doi.org/10.2110/jsr.2006.094

Cotterill, C.J., Phillips, E.R., James, L., Forsberg, C.F., Tjelta, T.I., Carter, G., Dove, D., 2017a. The evolution of the Dogger Bank, North Sea: A complex history of terrestrial, glacial and marine environmental change. Quat. Sci. Rev. 171, 136–153. https://doi.org/10.1016/j.quascirev.2017.07.006

Cotterill, C., Phillips, E.R., James, L., Forsberg, C.F., Tjelta, T.I., 2017b. How understanding past landscapes might inform present-day site investigations: A case study from Dogger Bank, southern central North Sea. Near Surf. Geophys. 15, 403–413. https://doi.org/10.3997/1873-0604.2017032

Cowell, P.J., Roy, P.S., Jones, R.A., 1991. Shoreface translation model: application to management of coastal erosion. Appl. Quat. Stud. 57–73.

Cowell, P.J., Thom, B.G., 1994. Morphodynamics of coastal evolution. Coast. Evol. Late Quat. Shorel. morphodynamics 33–86. https://doi.org/http://dx.doi.org/10.1017/CBO9780511564420.004

Dashtgard, S.E., MacEachern, J.A., Frey, S.E., Gingras, M.K., 2012. Tidal effects on the shoreface: Towards a conceptual framework. Sediment. Geol. 279, 42–61. https://doi.org/10.1016/j.sedgeo.2010.09.006

Davies, A.M., Furnes, G.K., 1980. Observed and Computed M2 Tidal Currents in the North Sea. J. Phys. Oceanogr. 10, 237–257. https://doi.org/10.1175/1520-0485(1980)010<0237:OACMTC>2.0.CO;2

Deschamps, P., Durand, N., Bard, E., Hamelin, B., Camoin, G., Thomas, A.L., Henderson, G.M., Okuno, J. ’ichi, Yokoyama, Y., 2012. Ice-sheet collapse and sea-level rise at the Bølling warming 14,600 years ago. Nature 483, 559–564. https://doi.org/10.1038/nature10902

Environment Agency, 2013. Coastal Morphology Report, Norfolk, Wells - Blakeney. Report – RP031/N/2013. Retrieved from https://www.channelcoast.org/anglia/analysis_programme/Coastal%20Morphology%20Report%20Wells%20to%20Blakeney%20Norfolk%20RP031N2013.pdf

Evans, D.J.A., Benn, D.I., 2004. A practical guide to the study of glacial sediments. Arnold.

Flinn, D., 1967. Ice front in the North Sea. Nature 215, 1151–1154. https://doi.org/10.1038/2151151a0

Forbes, D.L., Orford, J.D., Carter, R.W.G., Shaw, J., Jennings, S.C., 1995. Morphodynamic evolution, self-organisation, and instability of coarse-clastic barriers on paraglacial coasts. Mar. Geol. 126, 63–85. https://doi.org/10.1016/0025-3227(95)00066-8

Forbes, D.L., Taylor, R.B., Orford, J.D., Carter, R.W.G., Shaw, J., 1991. Gravel-barrier migration and overstepping. Mar. Geol. 97, 305–313. https://doi.org/10.1016/0025-3227(91)90122-K

Gardner, J. V., Calder, B.R., Hughes Clarke, J.E., Mayer, L.A., Elston, G., Rzhanov, Y., 2007. Drowned shelf-edge deltas, barrier islands and related features along the outer continental shelf north of the head of De Soto Canyon, NE Gulf of Mexico. Geomorphology 89, 370–390. https://doi.org/10.1016/j.geomorph.2007.01.005

Gardner, J. V., Dartnell, P., Mayer, L.A., Hughes Clarke, J.E., Calder, B.R., Duffy, G., 2005. Shelf-edge deltas and drowned barrier-island complexes on the northwest Florida outer continental shelf. Geomorphology 64, 133–166. https://doi.org/10.1016/j.geomorph.2004.06.005

Gibbard, P.L., Lewin, J., 2016. Filling the North Sea Basin: Cenozoic sediment sources and river styles.

Geol. Belgica 19, 201–217. https://doi.org/10.20341/gb.2015.017

Gibbard, P.L., West, R.G., Zagwijn, W.H., Balson, P.S., Burger, A.W., Funnell, B.M., Jeffery, D.H., de Jong, J., van Kolfschoten, T., Lister, A.M., Meijer, T., Norton, P.E.P., Preece, R.C., Rose, J., Stuart, A.J., Whiteman, C.A., Zalasiewicz, J.A., 1991. Early and early Middle Pleistocene correlations in the Southern North Sea basin. Quat. Sci. Rev. 10, 23–52. https://doi.org/10.1016/0277-3791(91)90029-T

Goff, J.A., Allison, M.A., Gulick, S.P.S., 2010. Offshore transport of sediment during cyclonic storms: Hurricane Ike (2008), Texas Gulf Coast, USA. Geology 38, 351–354. https://doi.org/10.1130/G30632.1

Graham, A.G.C., Stoker, M.S., Lonergan, L., Bradwell, T., Stewart, M.A., 2011. The pleistocene glaciations of the North Sea basin, in: Ehlers, J., Gibbard, P.L. (Eds.), Quaternary Glaciations – Extent and Chronology, 2nd Edition. Elsevier, pp. 261–278. https://doi.org/10.1016/B978-0-444-53447-7.00021-0

Green, A., Leuci, R., Thackeray, Z., Cooper, J.A.G., 2012. An overstepped segmented lagoon complex on the KZN continental shelf, South Africa 14, 13865. https://doi.org/10.4102/sajs.v108i7/8.969

Green, A.N., Cooper, J.A.G., Leuci, R., Thackeray, Z., 2013. Formation and preservation of an overstepped segmented lagoon complex on a high-energy continental shelf. Sedimentology 60, 1755–1768. https://doi.org/10.1111/sed.12054

Green, A.N., Cooper, J.A.G., Salzmann, L., 2018. The role of shelf morphology and antecedent setting in the preservation of palaeo-shoreline (beachrock and aeolianite) sequences: the SE African shelf. Geo-Marine Lett. 38, 5–18. https://doi.org/10.1007/s00367-017-0512-8

Gregoire, L.J., Payne, A.J., Valdes, P.J., 2012. Deglacial rapid sea level rises caused by ice-sheet saddle collapses. Nature 487, 219–22. https://doi.org/10.1038/nature11257

Hayes, M.O., 1979. Barrier island morphology as a function of tidal and wave regime, in: Leatherman, S.P. (Ed.), Barrier Islands. Academic Press, New York, pp. 1–27.

Hijma, M.P., Cohen, K.M., 2010. Timing and magnitude of the sea-level jump preluding the 8200 yr event. Geology 38, 275–278. https://doi.org/10.1130/G30439.1

Hijma, M.P., Engelhart, S.E., Törnqvist, T.E., Horton, B.P., Hu, P., Hill, D.F., 2015. A protocol for a geological sea-level database, Handbook of Sea-Level Research. John Wiley & Sons. https://doi.org/10.1002/9781118452547.ch34

Houbolt, J.J.H.C., 1968. Recent sediments in the southern bight of the North Sea. Geol. en Mijnb.

Hughes, A.L.C., Gyllencreutz, R., Lohne, ??ystein S., Mangerud, J., Svendsen, J.I., 2016. The last Eurasian ice sheets - a chronological database and time-slice reconstruction, DATED-1. Boreas 45, 1–45. https://doi.org/10.1111/bor.12142

IPCC, 2013. IPCC Fifth Assessment Report, IPCC.

Jansen, J.H.F., Van Weering, T.C., Eisma, D., 1979. Late Quaternary Sedimentation in the North Sea, in: The Quaternary History of the North Sea. Acta Universitatis, Symposium Universitatis Usaliensis Annum Quingentesinum Celebrantis, pp. 175–187.

Jarrett, B.D., Hine, A.C., Halley, R.B., Naar, D.F., Locker, S.D., Neumann, A.C., Twichell, D., Hu, C., Donahue, B.T., Jaap, W.C., Palandro, D., Ciembronowicz, K., 2005. Strange bedfellows - A deep-water hermatypic coral reef superimposed on a drowned barrier island; Southern Pulley Ridge, SW Florida platform margin. Mar. Geol. 214, 295–307. https://doi.org/10.1016/j.margeo.2004.11.012

Jensen, J.B., Stecher, O., 1992. Paraglacial barrier-lagoon development in the late pleistocene Baltic Ice Lake, southwestern Baltic. Mar. Geol. 107, 81–101. https://doi.org/10.1016/0025-3227(92)90070-X

Kelley, J.T., Belknap, D.F., Claesson, S., 2010. Drowned coastal deposits with associated archaeological remains from a sea-level “slowstand”: Northwestern Gulf of Maine, USA. Geology 38, 695–698. https://doi.org/10.1130/G31002.1

Kelsey, H.M., 2015. Geomorphological indicators of past sea levels, in: Handbook of Sea-Level Research. pp. 66–82. https://doi.org/10.1002/9781118452547.ch5

Kuchar, J., Milne, G., Hubbard, A., Patton, H., Bradley, S., Shennan, I., Edwards, R., 2012. Evaluation of a numerical model of the British-Irish ice sheet using relative sea-level data: Implications for the interpretation of trimline observations. J. Quat. Sci. 27, 597–605. https://doi.org/10.1002/jqs.2552

Leatherman, S.P., Rampino, M.R., Sanders, J.E., 1983. Barrier island evolution in response to sea level rise; discussion and reply. J. Sediment. Res. 53, 1026–1033. https://doi.org/10.1306/212F8314-2B24-11D7-8648000102C1865D

Lorenzo-Trueba, J., Ashton, A.D., 2014. Rollover, drowning, and discontinuous retreat: Distinct modes of barrier response to sea-level rise arising from a simple morphodynamic model. J. Geophys. Res. Earth Surf. 119, 779–801. https://doi.org/10.1002/2013JF002941

Matero, I.S.O., Gregoire, L.J., Ivanovic, R.F., Tindall, J.C., Haywood, A.M., 2017. The 8.2 ka cooling event caused by Laurentide ice saddle collapse. Earth Planet. Sci. Lett. 473, 205–214. https://doi.org/10.1016/j.epsl.2017.06.011

Mellett, C.L., Hodgson, D.M., Lang, A., Mauz, B., Selby, I., Plater, A.J., 2012. Preservation of a drowned gravel barrier complex: A landscape evolution study from the north-eastern English

Channel. Mar. Geol. 315–318, 115–131. https://doi.org/10.1016/j.margeo.2012.04.008

Mellett, C.L., Hodgson, D.M., Plater, A.J., Mauz, B., Selby, I., Lang, A., 2013. Denudation of the continental shelf between Britain and France at the glacial-interglacial timescale. Geomorphology 203, 79–96. https://doi.org/10.1016/j.geomorph.2013.03.030

Mellett, C.L., Plater, A.J., 2018. Drowned barriers as archives of coastal response to sea-level rise, in: Barrier Dynamics and Response to Changing Climate. pp. 57–89.

Menzies, J., 1990. Sand intraclasts within a diamicton mélange, southern Niagara Peninsula, Ontario, Canada. J. Quat. Sci. 5, 189–206. https://doi.org/10.1002/jqs.3390050303

Mitchum, R.M., Vail, P.R., Sangree, J.B., 1977. Seismic stratigraphy and global changes of sea level, Part six: stratigraphic interpretation of seismic reflection patterns in depositional sequences. Seism. Stratigr. — Appl. to Hydrocarb. Explor. 117–134. https://doi.org/10.1038/272400a0

Møller, I., Anthony, D., 2003. A GPR study of sedimentary structures within a transgressive coastal barrier along the Danish North Sea coast. Geol. Soc. London, Spec. Publ. 211, 55–65. https://doi.org/10.1144/gsl.sp.2001.211.01.05

Montreuil, A.L., Bullard, J.E., 2012. A 150-year record of coastline dynamics within a sediment cell: Eastern England. Geomorphology 179, 168–185. https://doi.org/10.1016/j.geomorph.2012.08.008

Moore, L.J., List, J.H., Williams, S.J., Stolper, D., 2010. Complexities in barrier island response to sea level rise: Insights from numerical model experiments, North Carolina Outer Banks. J. Geophys. Res. 115, F03004. https://doi.org/10.1029/2009JF001299

Moore, L.J., Murray, A.B., 2018. Barrier Dynamics and Response to Changing Climate. Springer International Publishing, Cham. https://doi.org/10.1007/978-3-319-68086-6

Mulhern, J.S., Johnson, C.L., Martin, J.M., 2017. Is barrier island morphology a function of tidal and wave regime? Mar. Geol. 387, 74–84. https://doi.org/10.1016/j.margeo.2017.02.016

Neill, S.P., Scourse, J.D., Bigg, G.R., Uehara, K., 2009. Changes in wave climate over the northwest European shelf seas during the last 12,000 years. J. Geophys. Res. 114, C06015. https://doi.org/10.1029/2009JC005288

Neill, S.P., Scourse, J.D., Uehara, K., 2010. Evolution of bed shear stress distribution over the northwest European shelf seas during the last 12,000 years. Ocean Dyn. 60, 1139–1156. https://doi.org/10.1007/s10236-010-0313-3

Novak, B., 2002. Early Holocene brackish and marine facies in the Fehmarn belt, southwest Baltic Sea: Depositional processes revealed by high-resolution seismic and core analysis. Mar. Geol. 189, 307–321. https://doi.org/10.1016/S0025-3227(02)00473-5

Oliver, T.S.N., Kennedy, D.M., Tamura, T., Murray-Wallace, C. V., Konlechner, T.M., Augustinus, P.C., Woodroffe, C.D., 2018. Interglacial-glacial climatic signatures preserved in a regressive coastal barrier, southeastern Australia. Palaeogeogr. Palaeoclimatol. Palaeoecol. #pagerange#. https://doi.org/10.1016/j.palaeo.2018.04.011

Orford, J.D., Murdy, J.M., Wintle, A.G., 2003. Prograded Holocene beach ridges with superimposed dunes in north-east Ireland: Mechanisms and timescales of fine and coarse beach sediment decoupling and deposition. Mar. Geol. 194, 47–64. https://doi.org/10.1016/S0025-3227(02)00698-9

Phillips, E., Hodgson, D.M., Emery, A.R., 2017. The Quaternary geology of the North Sea basin. J. Quat. Sci. 32, 117–126. https://doi.org/10.1002/jqs.2932

Phillips, E.R., Cotterill, C.J., Johnson, K., Crombie, K., James, L., Carr, S., Ruiter, A., 2018. Large-scale glacitectonic deformation in response to active ice sheet retreat across Dogger Bank (southern central North Sea) during the Last Glacial Maximum. Quat. Sci. Rev. 179, 24–47. https://doi.org/10.1016/j.quascirev.2017.11.001

Pretorius, L., Green, A., Cooper, A., 2016. Submerged shoreline preservation and ravinement during rapid postglacial sea-level rise and subsequent “slowstand.” Bull. Geol. Soc. Am. 128, 1059–1069. https://doi.org/10.1130/B31381.1

Rampino, M.R., Sanders, J.E., 1980. Holocene Transgression in South-Central Long Island, New York. SEPM J. Sediment. Res. Vol. 50, 1063–1079. https://doi.org/10.1306/212F7B7B-2B24-11D7-8648000102C1865D

Roberts, D.H., Evans, D.J.A., Callard, S.L., Clark, C.D., Bateman, M.D., Medialdea, A., Dove, D., Cotterill, C.J., Saher, M., Cofaigh, C.Ó., Chiverrell, R.C., Moreton, S.G., Fabel, D., Bradwell, T., 2018. Ice marginal dynamics of the last British-Irish Ice Sheet in the southern North Sea: Ice limits, timing and the influence of the Dogger Bank. Quat. Sci. Rev. 198, 181–207. https://doi.org/10.1016/j.quascirev.2018.08.010

Roep, T.B., Dabrio, C.J., Fortuin, A.R., Polo, M.D., 1998. Late highstand patterns of shifting and stepping coastal barriers and washover-fans (late Messinian, Sorbas Basin, SE Spain). Sediment. Geol. 116, 27–56. https://doi.org/10.1016/S0037-0738(97)00111-5

Roy, P.S., Cowell, P.J., Ferland, M.A., Thom, B.., 1994. Wave-Dominated Coasts, in: Coastal Evolution: Late Quaternary Shoreline Morphodynamics. Cambridge University Press, pp. 121–186.

Salzmann, L., Green, A., Cooper, J.A.G., 2013. Submerged barrier shoreline sequences on a high energy, steep and narrow shelf. Mar. Geol. 346, 366–374. https://doi.org/10.1016/j.margeo.2013.10.003

Sanders, J.E., Kumar, N., 1975. Evidence of shoreface retreat and in-place “Drowning” during holocene submergence of barriers, shelf off Fire Island, New York. Bull. Geol. Soc. Am. 86, 65–76. https://doi.org/10.1130/0016-7606(1975)86<65:EOSRAI>2.0.CO;2

Shaw, J., Fader, G.B., Taylor, R.B., 2009. Submerged early Holocene coastal and terrestrial landforms on the inner shelves of Atlantic Canada. Quat. Int. 206, 24–34. https://doi.org/10.1016/j.quaint.2008.07.017

Shennan, I., 1982. Interpretation of Flandrian sea-level data from the Fenland, England. Proc. Geol. Assoc. 83, 53–63. https://doi.org/10.1016/S0016-7878(82)80032-1

Shennan, I., Andrews, J., 2000. Holocene Land-ocean Interaction and Environmental Change Around the North Sea, Geological Society, London, Special Publications.

Shennan, I., Bradley, S., Milne, G., Brooks, A., Bassett, S., Hamilton, S., 2006. Relative sea-level changes, glacial isostatic modelling and ice-sheet reconstructions from the British Isles since the Last Glacial Maximum. J. Quat. Sci. https://doi.org/10.1002/jqs.1049

Shennan, I., Bradley, S.L., Edwards, R., 2018. Relative sea-level changes and crustal movements in Britain and Ireland since the Last Glacial Maximum. Quat. Sci. Rev. 188, 143–159. https://doi.org/10.1016/j.quascirev.2018.03.031

Shennan, I., Lambeck, K., Flather, R., Horton, B., McArthur, J., Innes, J., Lloyd, J., Rutherford, M., Wingfield, R., 2000. Modelling western North Sea paleogeographies and tidal changes during the Holocene, in: Holocene Land-Ocean Interaction and Environmental Change around the North Sea. Geological Society, London, Special Publications, pp. 299–319.

Stoker, M.S., Balson, P.S., Long, D., Tappin, D.R., 2011. An overview of the lithostratigraphical framework for the Quaternary deposits on the United Kingdom continental shelf 48.

Storms, J.E.A., Weltje, G.J., Terra, G.J., Cattaneo, A., Trincardi, F., 2008. Coastal dynamics under conditions of rapid sea-level rise: Late Pleistocene to Early Holocene evolution of barrier-lagoon systems on the northern Adriatic shelf (Italy). Quat. Sci. Rev. 27, 1107–1123. https://doi.org/10.1016/j.quascirev.2008.02.009

Storms, J.E.A., Weltje, G.J., van Dijke, J.J., Geel, C.R., Kroonenberg, S.B., 2002. Process-Response Modeling of Wave-Dominated Coastal Systems: Simulating Evolution and Stratigraphy on Geological Timescales. J. Sediment. Res. 72, 226–239. https://doi.org/10.1306/052501720226

Stride, A.H., 1959. On the Origin of the Dogger Bank, in the North Sea. Geol. Mag. 96, 33–44. https://doi.org/10.1017/S0016756800059197

Sturt, F., Garrow, D., Bradley, S., 2013. New models of North West European Holocene palaeogeography and inundation. J. Archaeol. Sci. 40, 3963–3976. https://doi.org/10.1016/j.jas.2013.05.023

Swift, D.J.P., 1975. Barrier-Island genesis: Evidence from the Central Atlantic Shelf, Eastern U.S.A. Sediment. Geol. 14, 1–43.

Swift, D.J.P., 1968. Coastal Erosion and Transgressive Stratigraphy. J. Geol. 76, 444–456.

Swift, D.J.P., Moslow, T.F., 1982. Holocene Transgression in South-Central Long Island, New York: DISCUSSION. SEPM J. Sediment. Res. Vol. 52, 1014–1019. https://doi.org/10.1306/212F80BC-2B24-11D7-8648000102C1865D

Swift, D.J.P., Phillips, S., Thorne, J.A., 1991. Sedimentation on continental margins, V: parasequences, in: Shelf Sand and Sandstone Bodies: Geometry, Facies and Sequence Stratigraphy. pp. 153–187. https://doi.org/10.1002/9781444303933.ch5

Tillmann, T., Wunderlich, J., 2013. Barrier rollover and spit accretion due to the combined action of storm surge induced washover events and progradation: Insights from ground-penetrating radar surveys and sedimentological data. J. Coast. Res. 65, 600–605. https://doi.org/10.2112/SI65-102.1

Törnqvist, T.E., Hijma, M.P., 2012. Links between early Holocene ice-sheet decay, sea-level rise and abrupt climate change. Nat. Geosci. 5, 601–606. https://doi.org/10.1038/ngeo1536

Uehara, K., Scourse, J.D., Horsburgh, K.J., Lambeck, K., Purcell, A.P., 2006. Tidal evolution of the northwest European shelf seas from the Last Glacial Maximum to the present. J. Geophys. Res. Ocean. 111, C09025. https://doi.org/10.1029/2006JC003531

van de Plassche, O., 1986. Sea-level research: a manual for the collection and evaluation of data. Springer Netherlands, Dordrecht. https://doi.org/10.1007/978-94-009-4215-8

Van Der Meer, J.J.M., Menzies, J., Rose, J., 2003. Subglacial till: The deforming glacier bed. Quat. Sci. Rev. 22, 1659–1685. https://doi.org/10.1016/S0277-3791(03)00141-0

van Heteren, S., Fitzgerald, D.M., Mckinlay, P.A., Buynevich, I. V., 1998. Radar facies of paraglacial barrier systems: coastal New England, USA. Sedimentology 45, 181–200. https://doi.org/10.1046/j.1365-3091.1998.00150.x

Ward, S.L., Neill, S.P., Scourse, J.D., Bradley, S.L., Uehara, K., 2016. Sensitivity of palaeotidal models of the northwest European shelf seas to glacial isostatic adjustment since the Last Glacial Maximum. Quat. Sci. Rev. 151, 198–211. https://doi.org/10.1016/j.quascirev.2016.08.034

Yang, B.C., Dalrymple, R.W., Chun, S.S., Lee, H.J., 2006. Transgressive sedimentation and stratigraphic evolution of a wave-dominated macrotidal coast, western Korea. Mar. Geol. 235, 35–48. https://doi.org/10.1016/j.margeo.2006.10.003

Zecchin, M., Catuneanu, O., 2013. High-resolution sequence stratigraphy of clastic shelves I: Units and bounding surfaces. Mar. Pet. Geol. 39, 1–25. https://doi.org/10.1016/j.marpetgeo.2012.08.015

Group (Stoker et al., 2011; Cotterill et al., 2017a)	Formation	Age	Subdivisions (Cotterill et al., 2017a)	Sedimentary environment	Description in Tranche B (Cotterill et al., 2017a)
California Glaciogenic Group	Nieuw Zeeland Gronden Formation	Holocene, MIS 1 Present day - ~ 6000 BP	Terschellinger Bank Member	Shallow marine	Bioturbated marine sands
	Elbow Formation	Holocene, MIS 1 ~11000 BP – ~6000 BP		Estuarine, intertidal	Mudflats, some transgressive sands.
	unnamed	Late Pleistocene, MIS 2 ~17500 BP to ~11000 BP		Periglacial, sandur and glaciofluvial outwash	Not formally recorded within other Formations. Well sorted sands, evidence for cryoturbation. Extensive river networks exist in seismic reflection data.
	Botney Cut Formation	Late Pleistocene, MIS 2 ?deglacial stage, ~21000 BP to ~17500 BP		Proglacial	Found in an intra-moraine basin as rhythmically-laminated silts and very fine sands with rare dropstones, interpreted to be proglacial lake deposits.
	Dogger Bank Formation	Late Pleistocene, MIS 2-4 ~70000 BP - ~17500 BP	Younger Dogger Bank 1 Transition 1 Younger Dogger Bank 2 & 3 Transition 2 Older Dogger Bank 1, 2 & 3 Basal Dogger Bank	Glacial and periglacial	Upper units encountered in this study: matrix-supported diamict with chalk and flint, sand pods and intraclasts, and often showing micromorphology suggesting subglacial deformation (Carr et al., 2006), often glaciotectonised into arcuate ridges interpreted to be terminal moraines related to ice margin oscillation (Cotterill et al., 2017a; Phillips et al., 2018).

Table 1. Simplified stratigraphy of Dogger Bank based on Stoker et al., 2011; Cotterill et al., 2017a. The location of Tranche B of the Forewind site is shown on Figure 2.

Lithofacies code (Evans and Benn, 2004)	Short description	Munsell colour	Grain size	Sedimentary structures	Other notes
Sm_1	Massive, bioturbated sand	Dark greyish brown 2.5Y 4/2, olive brown 2.5Y 4/3	Fine to very fine sand (Φ 3-4)	Massive, structureless	Mottled colouring. Abundant disarticulated shells and shell fragments (<10 mm).
Gms	Matrix-supported gravel	Greyish brown 2.5Y 5/2	Medium sand Φ 2 with clasts from very coarse sand (Φ 0) to very large pebbles (Φ -6)	Massive, structureless	Clasts are subrounded to rounded, occasionally sub-angular, consisting of limestone, chalk, red sandstone and gneiss.
Sl	Laminated sand	Grey 2.5Y 6/1 with dark grey 2.5Y 4/1 laminations	Fine sand (Φ 3-2)	Laminated	Well sorted, clean sand, very high quartz content. Some thin peat (Fpt) layers up to 2 mm thick. Some shell fragments.
Fm	Massive silt/clay with sand laminations	Dark grey 5Y 4/1, dark greyish brown 10YR 4/2 with olive brown 2.5Y 4/3, greyish brown 2.5Y 5/2 laminations	Clay and silty clay. Laminations of fine sand (Φ 2) with coarser, poorly sorted laminations from fine sand (Φ 2) to granules (Φ -1).	Massive with basal laminations in core 214. Sand laminae throughout, with evidence of erosion.	Also contains thin, silty peats (Fpt) up to 5 mm thick.
Sm_2	Massive sand with peat chips	Light brownish grey 2.5Y 6/2	Fine sand (Φ 3)	Massive, structureless	Contains peat chips, clasts and stringers. Amount of allochthonous peat increases towards base of lithofacies.
Fpt	Silt/clay peat	Black 2.5Y 2.5/1	Clay and silty clay	Massive, structureless	Rootlets with iron-stained nodules. Previous authors' foraminiferal analysis found *Jadaminna macrescens* and *Trochaminna inflata* (Shennan et al., 2000).
Sd	Deformed sand	Dark greyish brown 2.5Y 4/2, light olive brown 2.5Y	Fine sand (Φ 3) and very fine sand (Φ 4)	Various forms of deformation	Starry-night textures, recumbent folds, ball-and-pillow, loading, and dewatering structures are observed

		5/3, light yellowish brown 2.5Y 6/3, light olive grey 5Y 6/2			
Dmm	Matrix-supported diamict	Brown 10YR 4/3	silty clay to very large pebbles (Φ -6)	Massive, structureless	Stiff. Clasts angular to subrounded, predominantly subangular, consisting of flint, chalk, limestone, red sandstone, microgranite, gneiss. Rip-up clasts and inclusions of sand.

Table 2. Lithofacies observed in vibrocores shown in Figure 4. Photograph examples of each lithofacies are shown in Figure 5.

Seismic unit	*Horizon*	Amplitude	Frequency	Continuity	Configuration	Termination	Geometry	Thickness
SU-H		Transparent	-	Discontinuous	-	Concordant	Wedge	Up to 0.016 s (~13 m)
SU-G		High	High	Continuous	Even parallel	Truncation	Sheet	Approximately two reflectors maximum (0.0006 s, ~50 cm)
	S2	*High*		*Continuous*			*Unconformity*	
SU-F		High	Medium to high	Discontinuous	Tangential oblique to complex sigmoid-oblique	Downlap	Lens	Maximum 0.0035 s (~2.8 m)
SU-E		Transparent	-	Discontinuous	-	Onlap or concordant	Wedge or lens	Up to 0.005 s (~4 m)
SU-D		Transparent	-	Discontinuous	-	Erosive	Channel	0.001 s (~0.8 m) to 0.008 s (~6.4 m)
SU-C		High	High	Continuous	Mildly divergent	Onlap or concordant	Drape/wedge	Up to 0.0004 s (~30 cm)
SU-B		Transparent, medium or high	Low	Discontinuous	Transparent, shingled to sigmoidal	Concordant or downlap	Mound	Up to 0.004 s (~3.3 m)
	S1	*High*		*Continuous*			*Unconformity*	
SU-A		Transparent or low	Low	Discontinuous	Chaotic	-	Basal	-

Table 3. Seismic facies observed in pinger seismic reflection data. Seismic units are shown on Figure 7.

Seismic stratigraphic unit	*Horizon*	Lithofacies	Interpreted depositional environment	Stratigraphic unit
SU-H		Sm_1	Lower shoreface to offshore	Shallow marine
SU-G		Gms	Transgressive gravel lag	
	S2			*Composite flooding surface and wave ravinement surface (Cattaneo and Steel, 2003)*
SU-F		Sl	Back-barrier beach	Barrier phase B
SU-E		Fm	Tidal mudflat	Back barrier
		Fpt	Salt marsh	
SU-D		Not penetrated	Tidal creek	
SU-C		Sm_2	Washover fan	
SU-B		Not penetrated	Barrier	Barrier phase A
	S1			*Transgressive surface (Cattaneo and Steel, 2003)*
SU-A		Dmm	Subglacial	Pre-Holocene basement
		Sd	Glacial outwash plain and glaciofluvial, periglacially-deformed	

Table 4. Lithofacies, seismic unit and depositional unit relationships.

Forcing	RSL rise (Kuchar et al., 2012)	Tidal regime (Uehara et al., 2006; Ward et al., 2016)	Wave regime (Neill et al., 2009)	Ravinement depth/FWWB	Storminess
phase A	11-9 mm/year	Mesotidal (2-4 m)	Low energy	Shallow	Unknown (no core evidence)
phase B	10 mm/year	Micro-mesotidal (1-3 m)	Higher energy than phase A	Deeper	High (frequent high-energy events in tidal mudflats)

Inertia	Grain size (Fig. 4)	Sediment supply	Average slope (Fig. 7)	Relative topographic complexity (Fig. 7)	Back-barrier length (Fig. 7 and 8)
phase A	Unknown (coarse?)	High	0.017°	Low (flat)	~1.5 km
phase B	Fine sand	High	0.046°	High (channels and basement highs)	~1 km

High
Medium
Low

Table 5. Summary of factors affecting barrier forcing and inertia during each barrier phase. Colours correspond to low, medium or high factors of forcing and inertia.

Figure captions

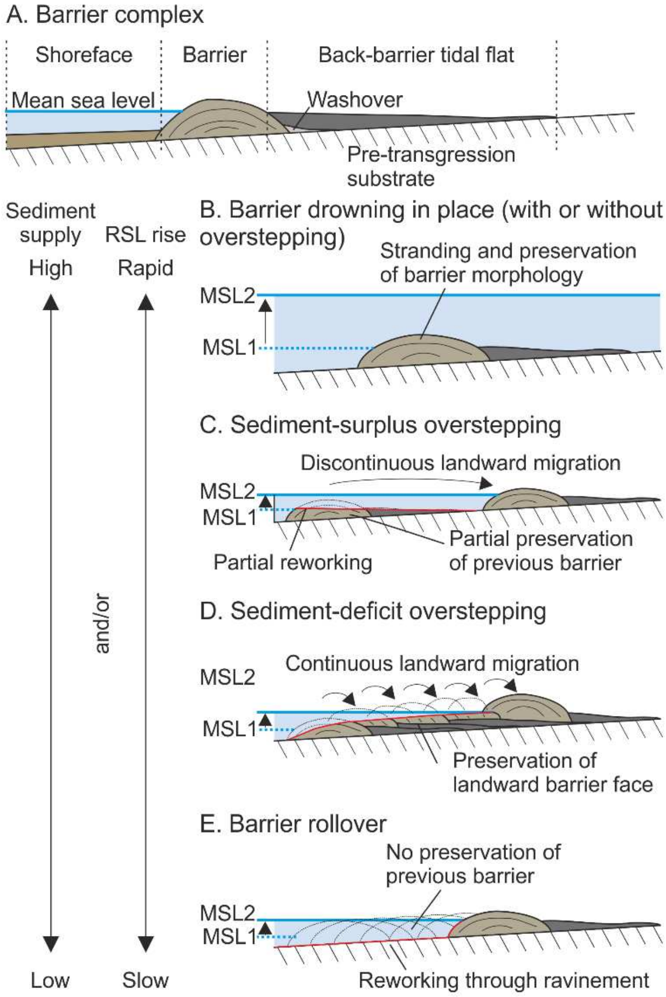

Fig. 1. Summary of barrier retreat during relative sea-level (RSL) rise under simplified, relative comparison of available sediment supply and rate of RSL rise, adapted from Mellett et al. (2012) A. Geomorphology and sedimentary environments of a typical barrier system. B. Drowned in place barrier. As sea level rises rapidly from MSL1 to MSL2, the barrier undergoes minimal reworking and its morphology is preserved, leaving the barrier stranded. A new barrier may initiate landward through sediment-surplus overstepping but is not necessary for in-place drowning. C. Sediment-surplus overstepping. Landward migration of the barrier with partial reworking and partial preservation (or in-place drowning) of the MSL1 barrier. Migration to the MSL2 barrier is a discontinuous overstep to a new landward location without requiring reworking of the entire previous barrier to initiate the new barrier. D. Sediment-deficit overstepping. Lower sediment supply under rapid RSL rise leads to continuous overstepping from continual reworking of the previous barrier. E. Barrier rollover. The barrier is entirely reworked to provide the sediment to sustain the new barrier location.

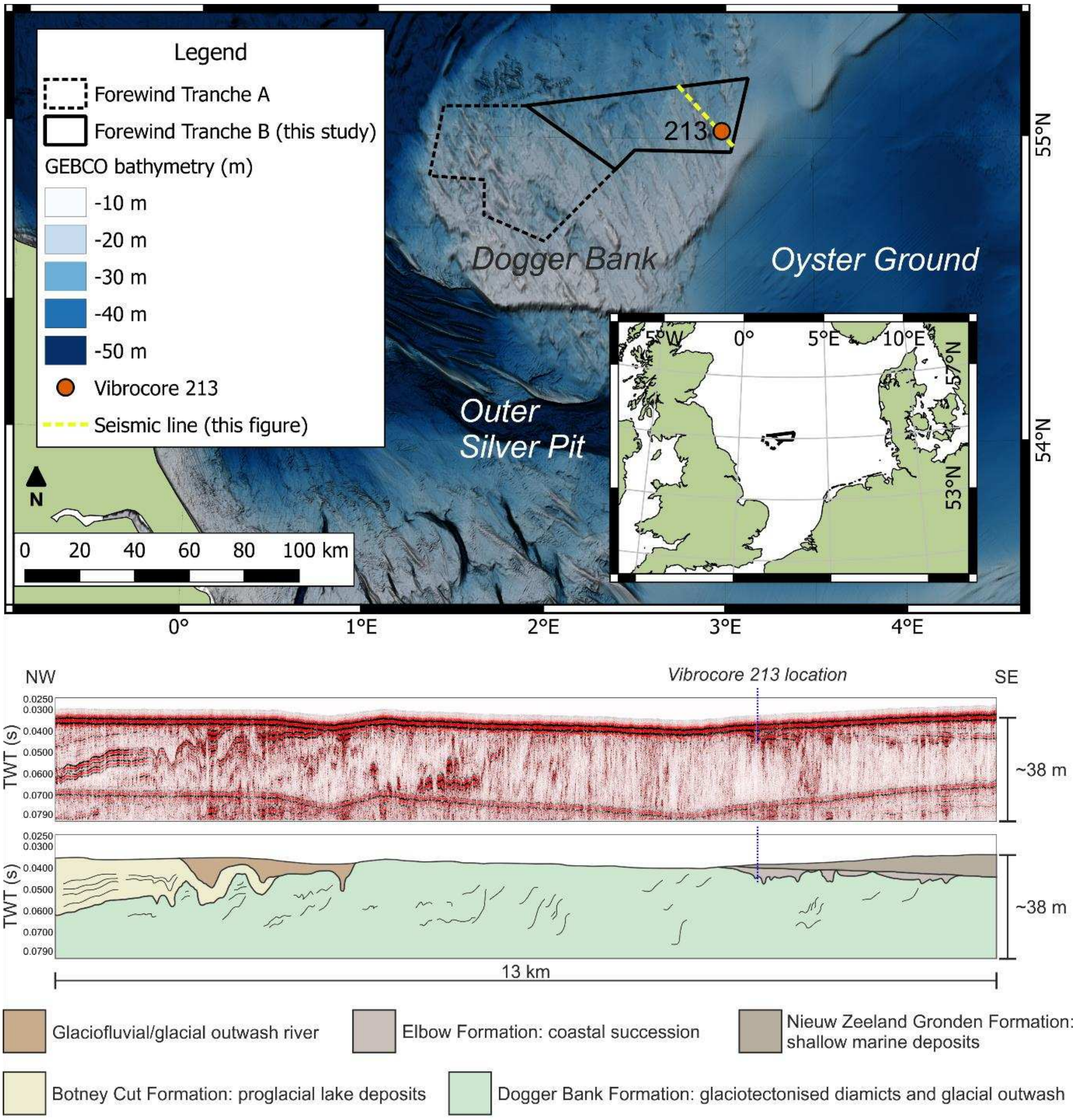

Fig. 2. Location of Dogger Bank in the Southern North Sea showing the locations of the Forewind project Tranche A (dotted outline) and Tranche B, the focus for this study (solid outline) as well as vibrocore 213 and other locations given in the text. The sparker-source seismic section shows the stratigraphic context of coastal deposits preserved at Dogger Bank. Bathymetry data from GEBCO (https://www.gebco.net).

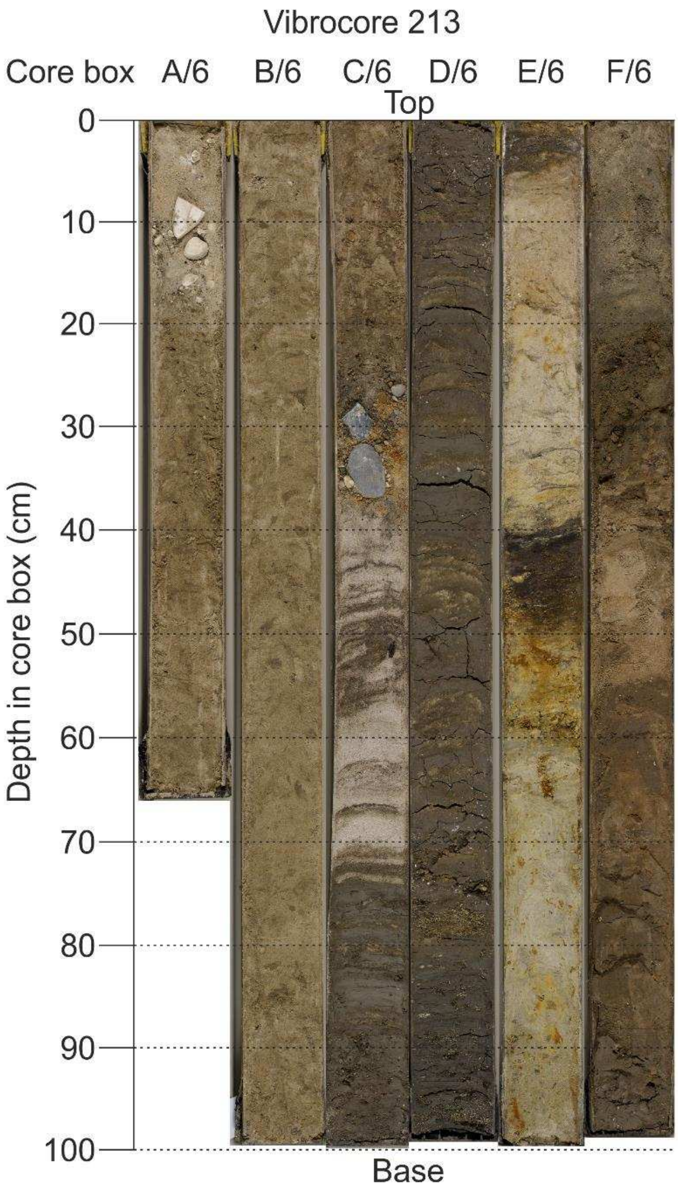

Fig. 3. Uninterpreted photograph of vibrocore 213 (photo date August 2017, core acquired July 1994) showing contrast and variation in lithofacies interpreted.

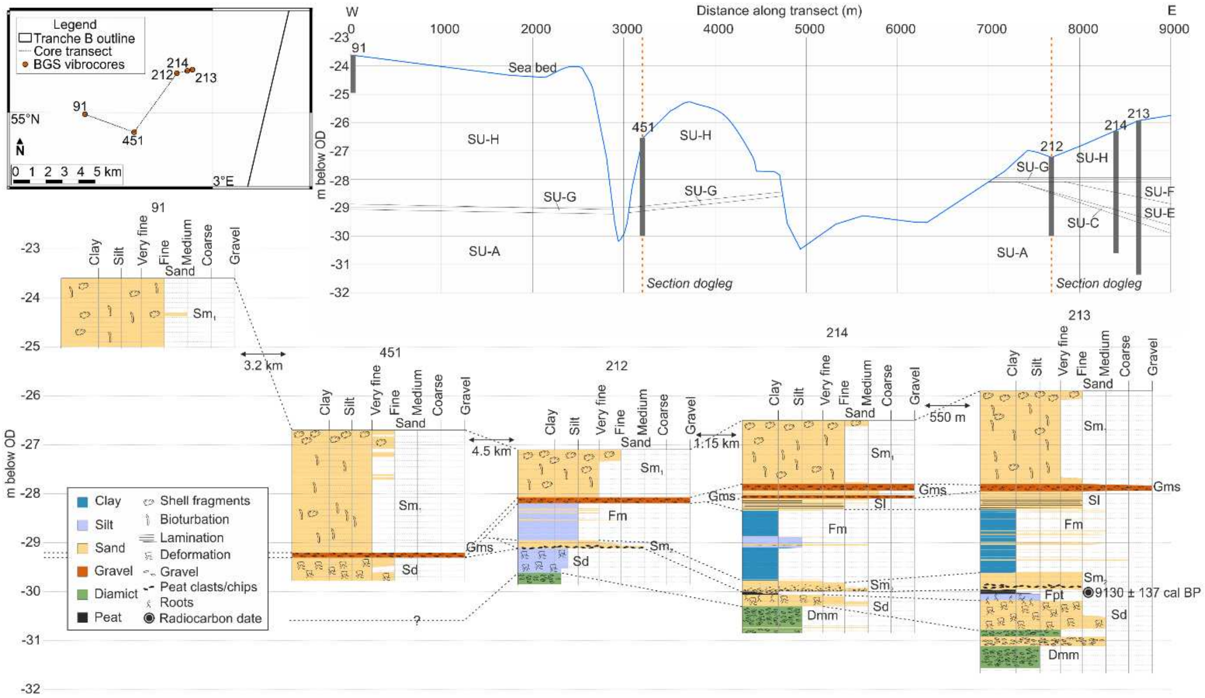

Fig. 4. Core transect through vibrocores in the southeast of Tranche B showing correlation between lithostratigraphy and seismic units. The top section shows the true horizontal separation between each vibrocore, as well as the approximate, simplified seismic units (SU). The bottom section shows correlation between lithofacies in each vibrocore. Lithofacies codes are explained in Table 2 and shown in Figure 5. Seismic units are explained in Table 3 and shown in Figure 6 and 7.

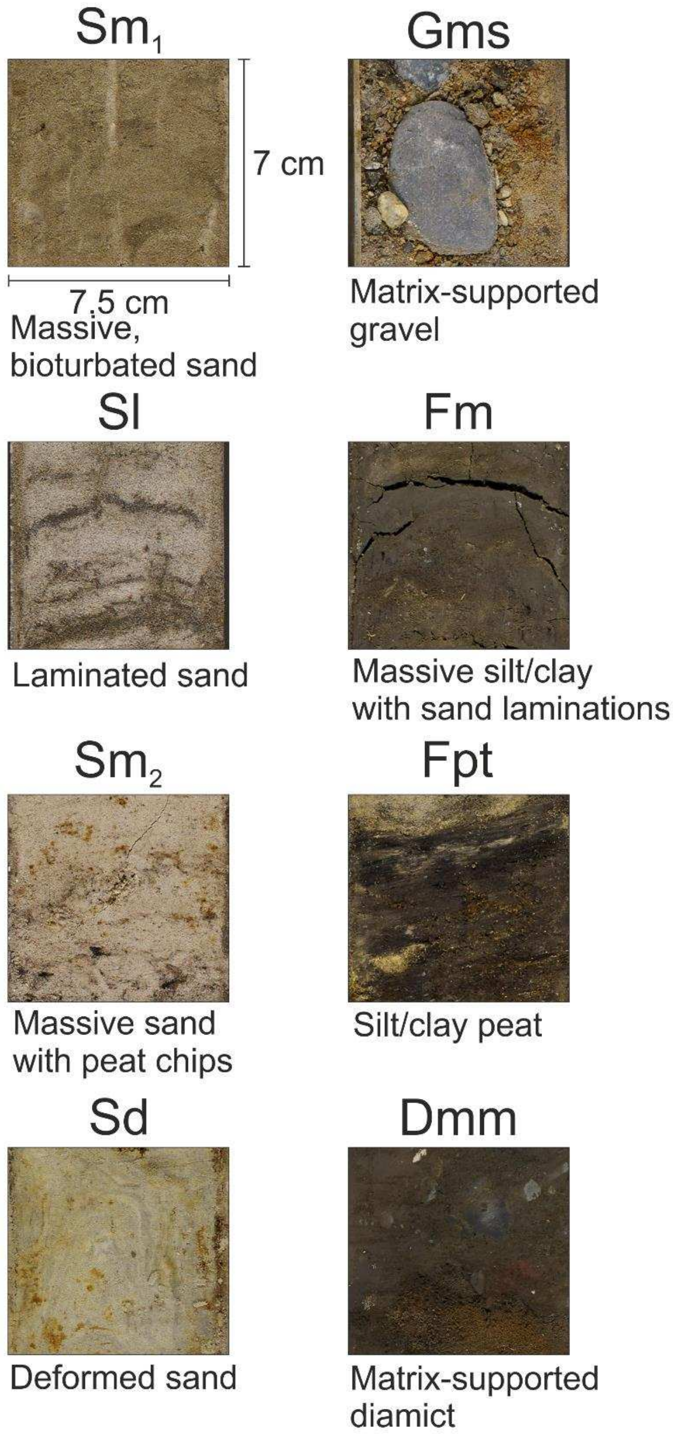

Fig. 5. Photographs of the eight lithofacies observed in vibrocores. Short descriptions of each lithofacies are given in Table 2.

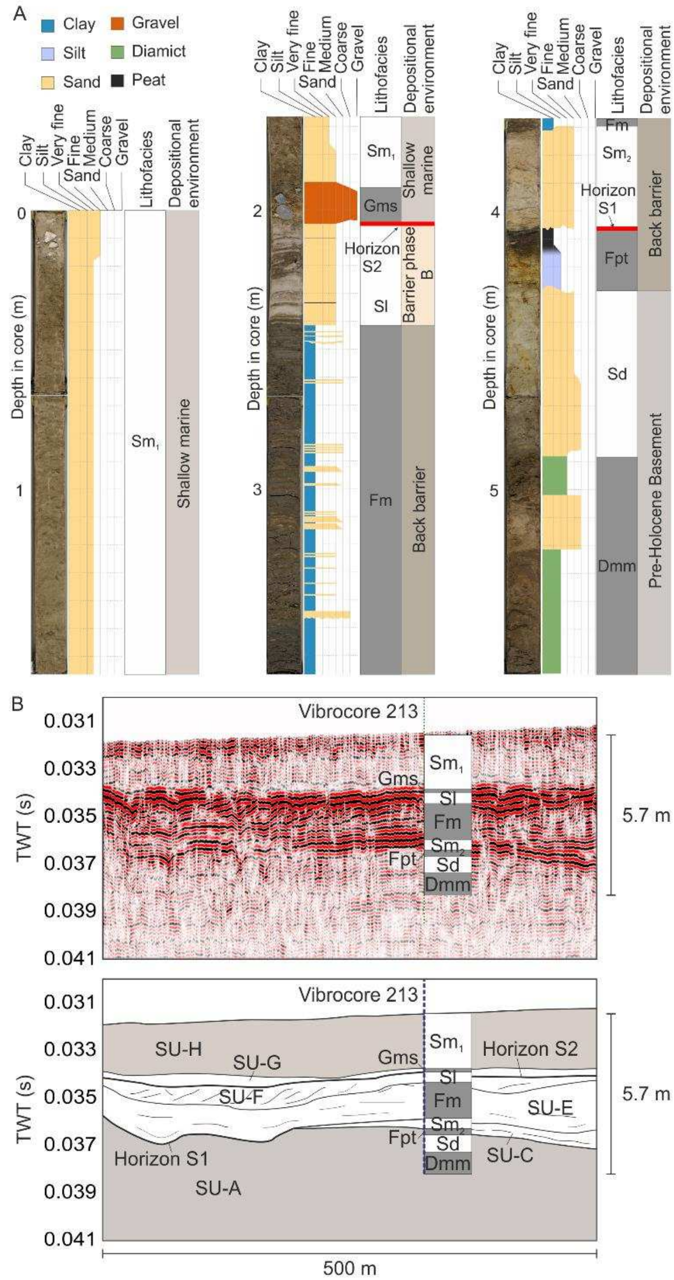

Fig. 6. Calibration between vibrocore and pinger-source seismic reflection data. A. Vibrocore 213 uninterpreted photographs, core log, lithofacies, key seismic horizons and interpreted depositional environment. B. Vibrocore 213 lithofacies compared to pinger seismic reflection data showing calibration to seismic units. Seismic data are shown in two-way travel time (TWT) and vibrocore depth has been converted to TWT using an average velocity of 1600 ms^{-1} as given by Cotterill et al. (2017b).

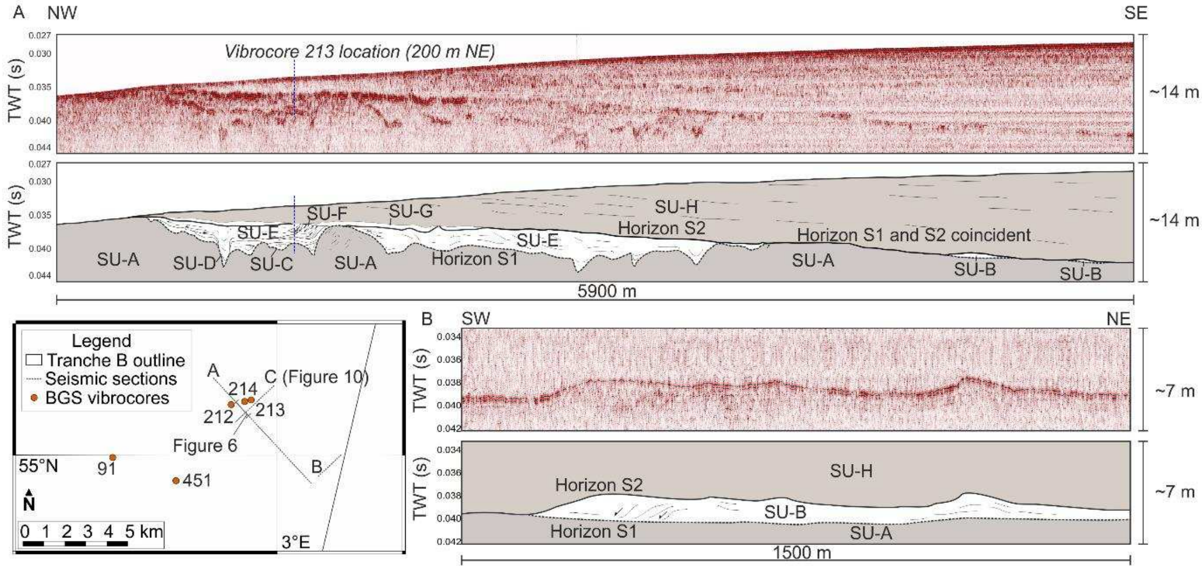

Fig. 7. Pinger-source seismic section showing the stratigraphy and character of observed seismic units. Further examples of seismic units are shown in Figures 6 and 10. Seismic units are described in Table 3.

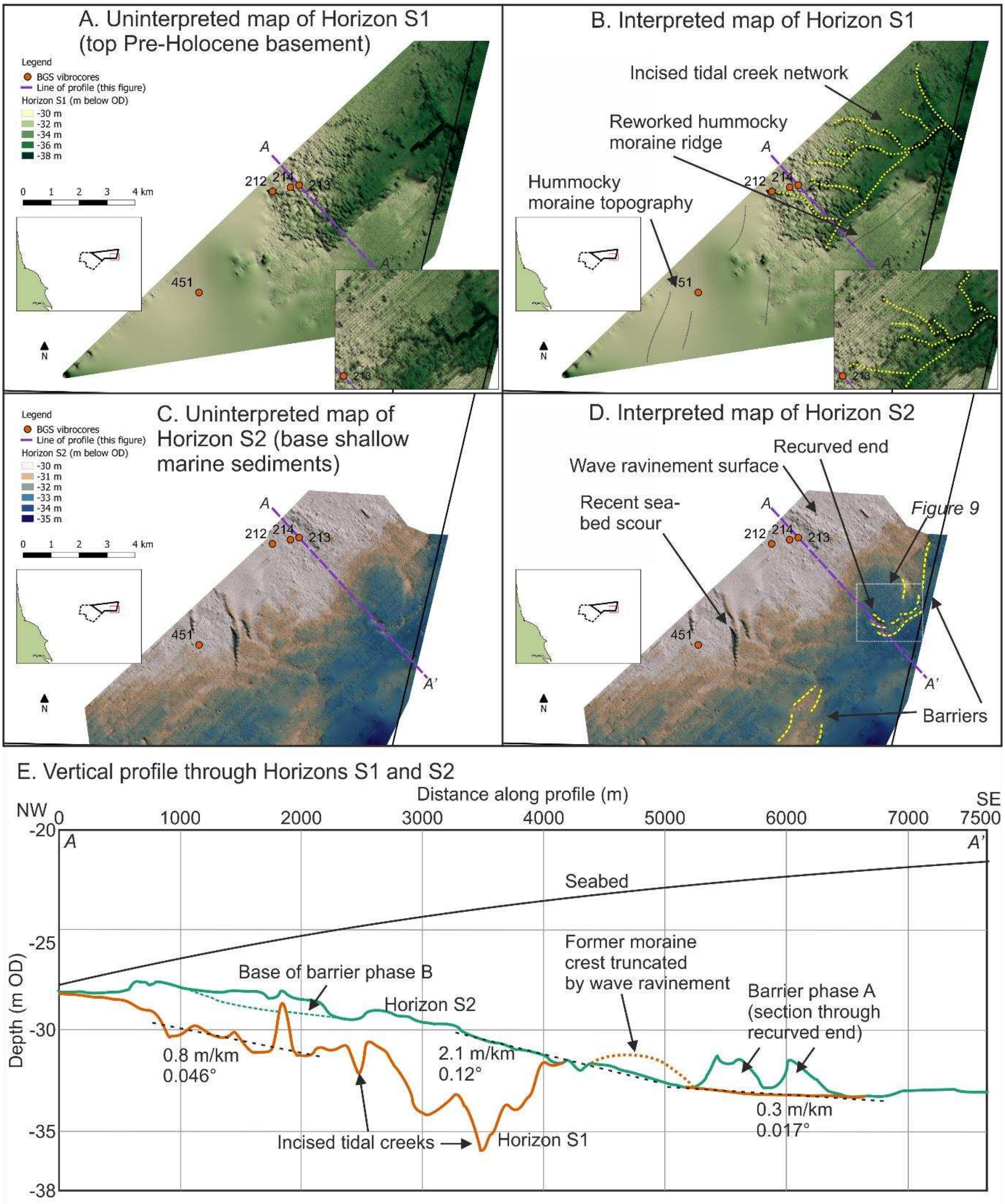

Fig. 8. Maps and vertical section showing the main surfaces mapped from pinger-source seismic data. A. Uninterpreted and B. interpreted maps of horizon S1 showing the nature of the antecedent topography and channel network. Insets show the same surface mapped from the sparker-source seismic data, with a lower vertical and horizontal resolution, but a higher depth of investigation, resulting in some clarification of the channel network. C. Uninterpreted and D. interpreted maps of horizon S2 showing the mound geometry of barrier phase A. E. Vertical section through horizons S1

and S2 showing key average gradients (values of the dashed line in degrees and m/km), and geomorphological features.

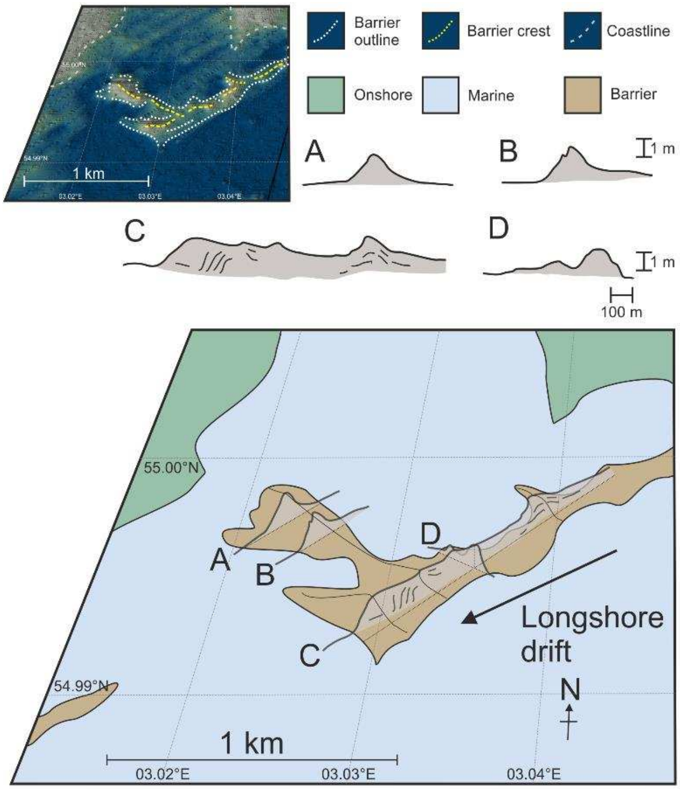

Fig. 9. Fence diagram showing interpretation of the preserved barrier phase A. Pinger-source seismic sections were used to create a 3D reconstruction of barrier morphology, shown in relation to longshore drift direction.

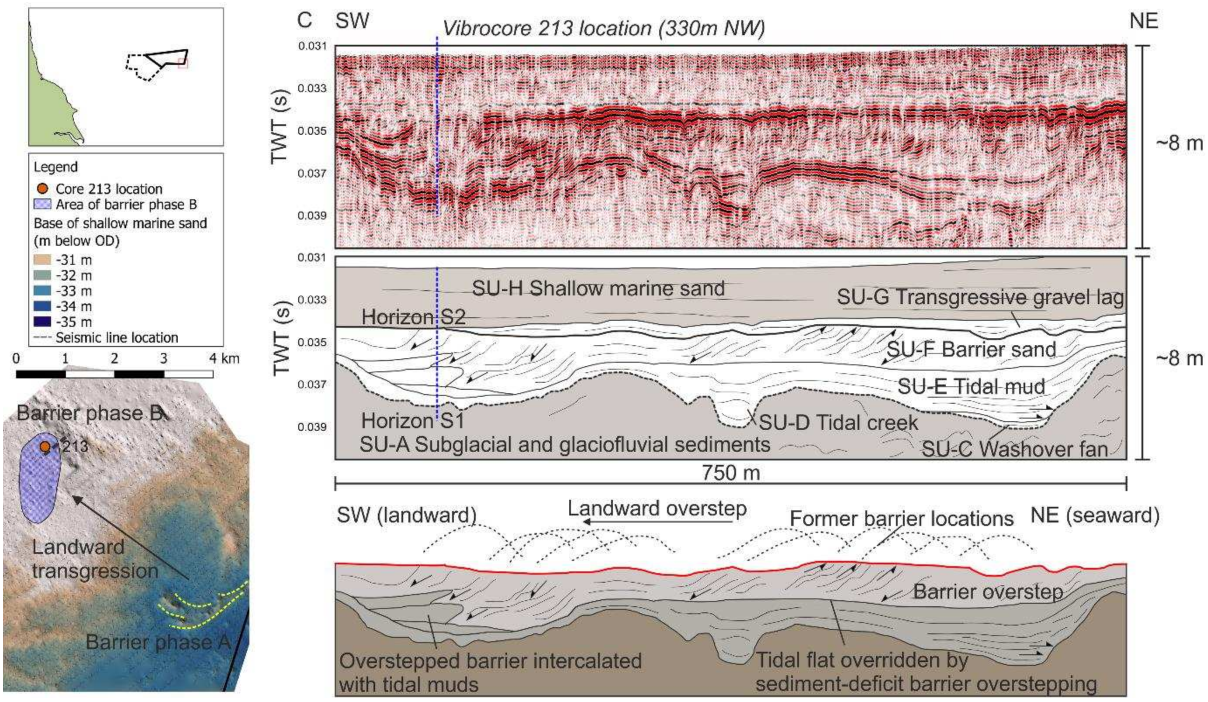

Fig. 10. Pinger-source seismic section showing barrier phase B seismic units. Landward-dipping oblique to sigmoidal reflectors in the barrier sand downlapping onto tidal mudflats imply landward barrier overstepping.

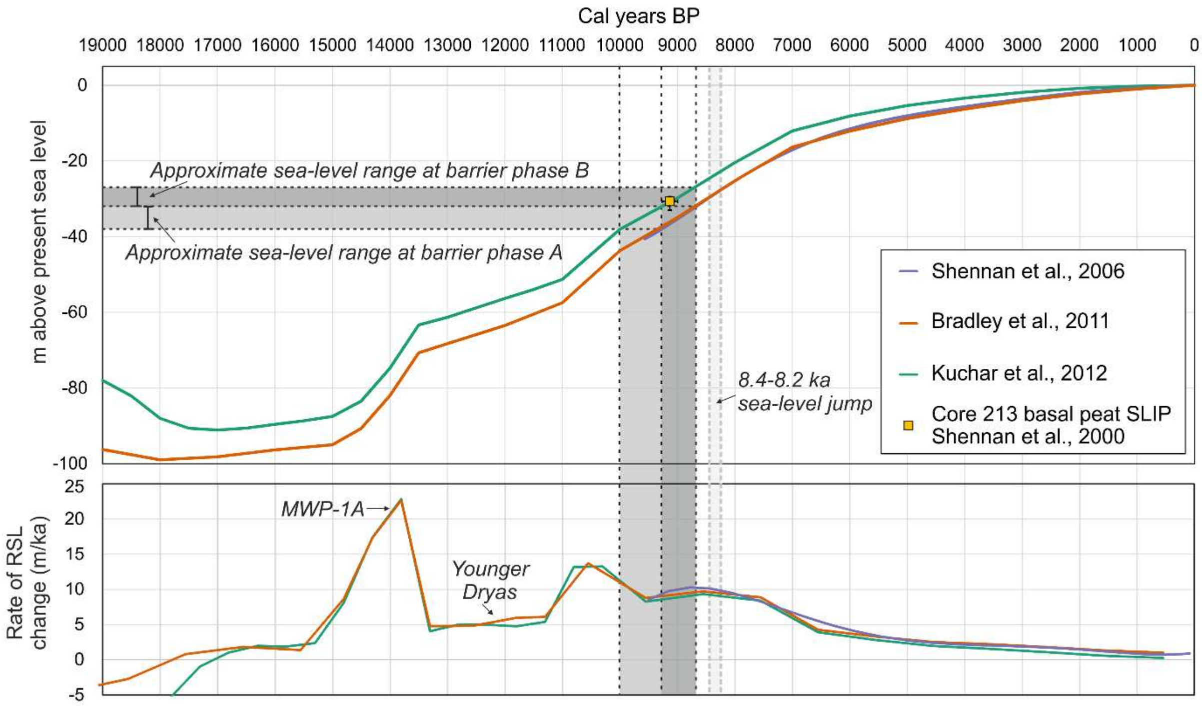

Fig. 11. RSL curves from GIA models (Shennan et al., 2006; Bradley et al., 2011; Kuchar et al., 2012), top, shown with the rate of RSL change (bottom curves). The sea-level index point from Shennan et al. (2000) is also shown. The elevations of barrier phases A and B are shown for comparison to RSL. Also highlighted is the 8.4-8.2 ka sea-level jump that occurred after the presence of barrier phase B.

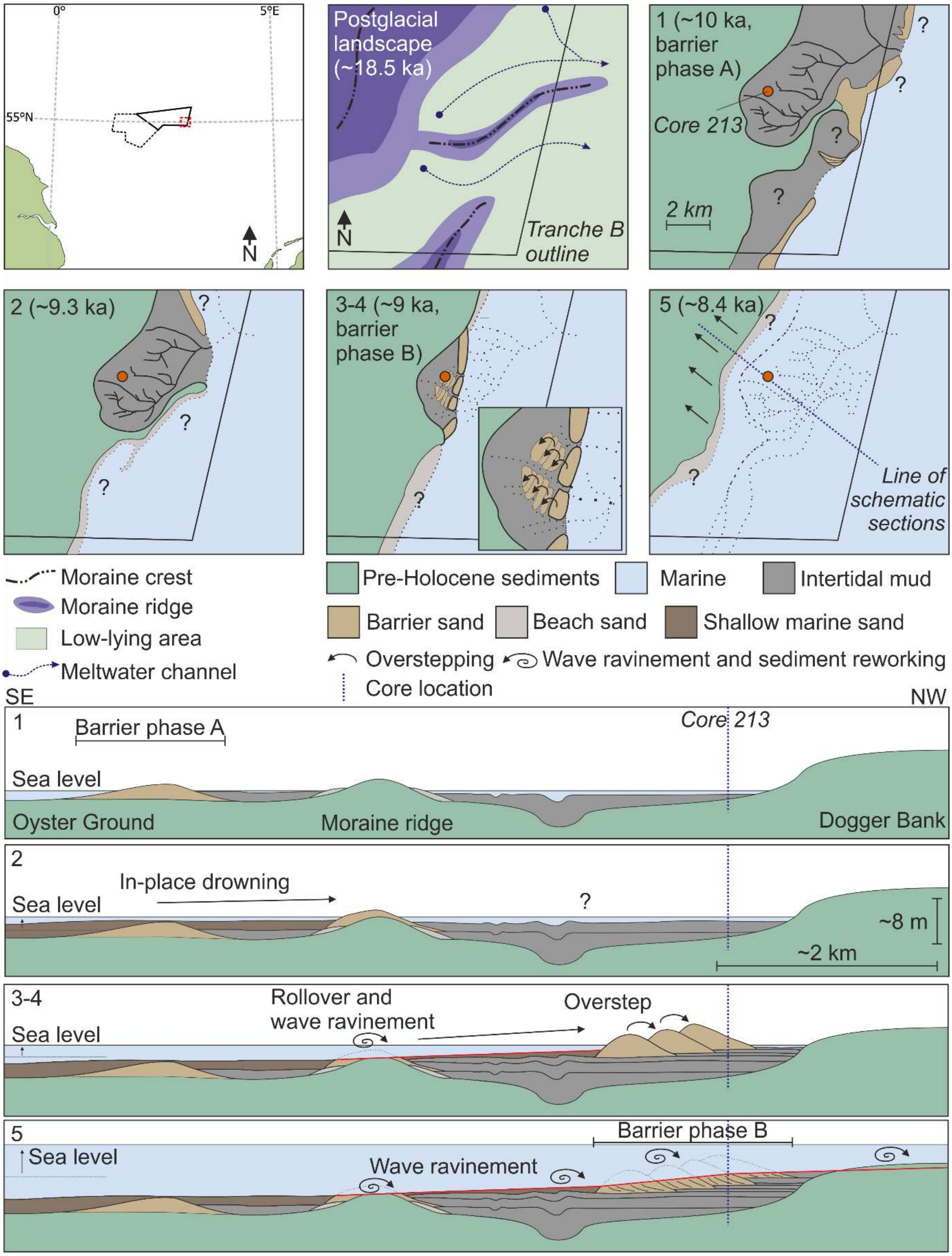

Fig. 12. Model maps and schematic sections of landscape evolution from initial postglacial landscape to Holocene transgression, showing barrier initiation and migration in response to rapid RSL rise. Numbers 1-5 refer to coastal evolution stages as discussed in Section 4.4 of the main text.

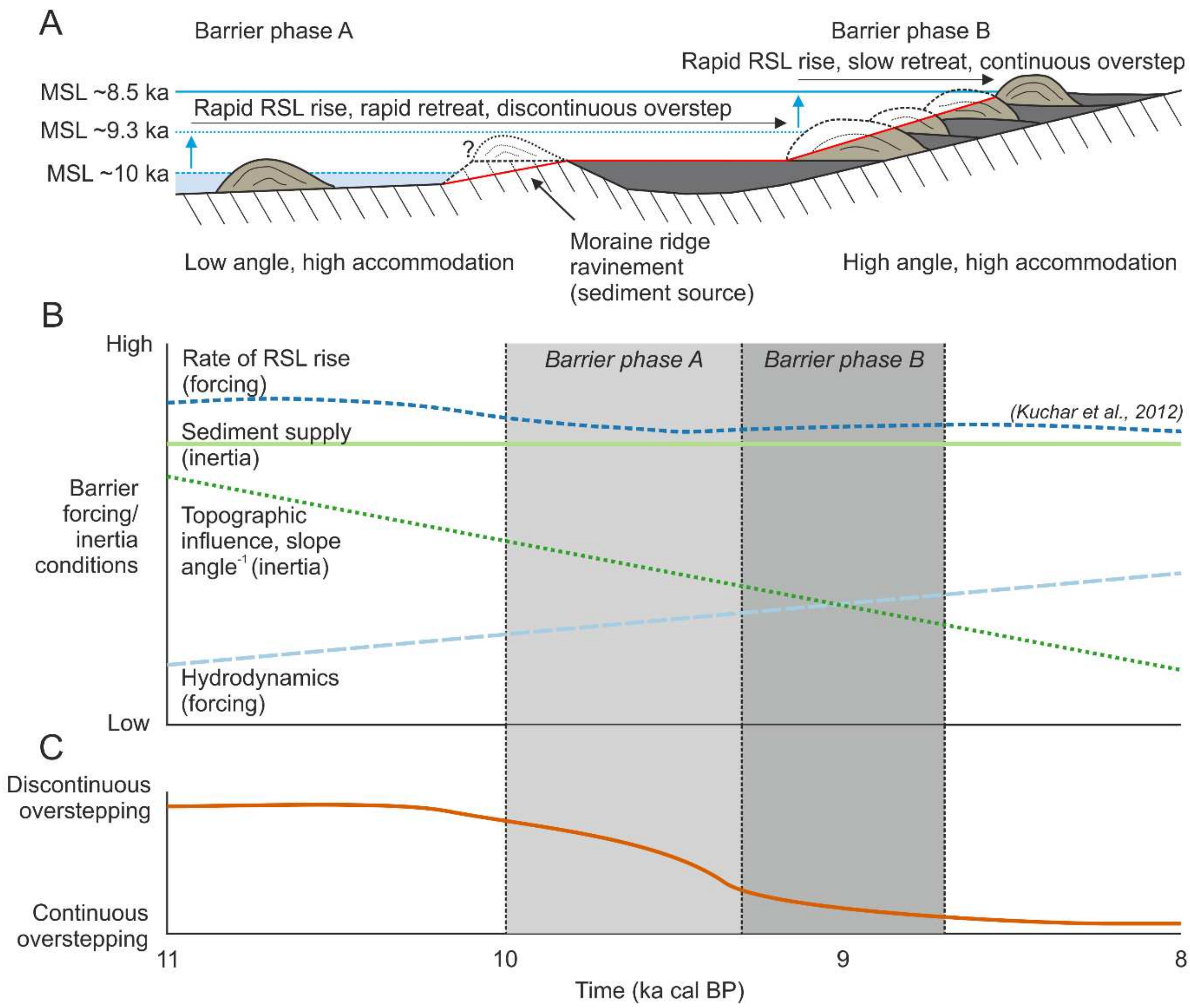

Fig. 13. Summary model of barrier retreat mechanisms in response to complex antecedent topography and changing slope. A. Cross-sectional model showing barrier response to forcing and inertia conditions at Dogger Bank. The red line represents wave ravinement. B. Qualitative summary of barrier forcing and inertia conditions through time. RSL rise comes from Kuchar et al. (2012). Other curves are qualitatively derived from observations in seismic mapping and from tidal and wave modelling (Neill et al., 2009; Uehara et al., 2006; Ward et al., 2016) C. Resulting retreat mechanism as a combination of forcing and inertia conditions changing through time. Retreat changes from discontinuous and laterally rapid to continuous and laterally slower.